University of Nottingham
UK | CHINA | MALAYSIA

Understanding Active Galactic Nuclei activity through infrared variability and host galaxy decomposition in the Ultra Deep Survey

Karel Green

Thesis submitted to the University of Nottingham
for the degree of Doctor of Philosophy

March 2024

I am, somehow, less interested in the weight and convolutions of Einstein's brain than in the near certainty that people of equal talent have lived and died in cotton fields and sweatshops.

— Stephen Jay Gould, The Panda's Thumb: More Reflections in Natural History

For my mum, dad and sister.

Thank you for ensuring I was always doing something but never caring what it was. Your gentle encouragement lead me beyond the stars.

Abstract

Please give a brief overview of your thesis here.

Acknowledgements

Acknowledgements here

List of Publications

1. Your First Publication [Chapter 3]
2. Your Second Publication [Chapter 4]
3. Your Third Publication [Chapter 5]
4. Your Forth Publication [Chapter 6]

   ...

Contents

List of Tables

List of Figures

Chapter 1

Introduction

1.1 Models of the universe

One of the foremost goals of astrophysical research is to understand how the universe evolved to appear as it does today. Throughout history there have been many models of the structure and extent of the cosmos, with western views first assuming the Earth was all their is to the world, moving on to discover the rest of our solar system through a geocentric lens until finally realising that the movement of the planets on the sky are better explain by the heliocentric model.

However this still was not 100% correct as we now know that though the planets do revolve around The Sun, The Sun is not, in fact, at the centre of the universe. Further research found that we exist within a galaxy made up of many other objects, similar and different to our own world. Other planets and stars that combine to make solar systems as well as dust and gas, all revolving around an invisible point of infinite density we call a black hole.

The great debate finally put to rest the idea that The Milky Way is alone and the sum total of the universe, with observations confirming the existence of other objects far beyond the limits of our own galaxy and that they were galaxies in their own right. This prompted a new age in astrophysics, with extra-galactic studies taking off into a sub-field of it's own as scientists tried

to understand how and why these objects exist.

1.2 Extragalactic Astrophysics

Many observations and trends have been found since the discovery that the universe contains many galaxies, most notably it was discovered that not all galaxies are the same.

First observed in [Fill this out later]active galactic nuclei (AGN) we described as being bright points in the centres of some galaxies.

1.3 Active Galactic Nuclei

1.4 Paper 1 Introduction

Active Galactic Nuclei (AGN) activity has long been observed within the Universe and is characterised by its dynamic multi-wavelength emission that spans the entire electromagnetic spectrum [1]. The immense radiation produced in AGN systems is one of the most powerful phenomena in the known universe and is theorised to arise from accretion of material onto a central supermassive black hole [2].

The effects this emission provides is crucial to our understanding of the Universe and how it evolved to it's current state, with active galaxies being major elements in both the early and present-day universe. Simulations, for example, find the powerful radiation to be a key factor in reproducing observed re-ionisation [3], furthermore many relations between black holes and their host galaxies have been reported (e.g. $M_{BH} - \sigma_*$, $M_{BH} - M_{Bulge}$ and the BH accretion rate - cosmic star formation rate correlation; see **(author?)** 4 for a review) indicating some level of co-evolution of AGN and their host galaxy through to the present day universe where the cooling flow problem in large scale, cluster environments is attributed to their outflows [5].

Despite their many scientific uses, interesting effects and abundance in the universe, AGN activity - and the underlying mechanisms behind it - is still not fully understood.

Due to the small physical size of black holes, accretion and emission from AGN occurs on scales many orders of magnitude smaller than that of a galaxy, and therefore quickly becomes difficult to resolve with increasing redshift [6].

Unpicking it's emission from that of the host galaxy also poses a large barrier in understanding the structure and impacts of the accretion process (**(author?)** 7; **(author?)** 8; **(author?)** 9; **(author?)** 10) and there is no formal consensus on the trigger (or triggers) that activates AGN in the galaxies that are active. Multiple ideas are present within the literature, finding evidence for (**(author?)** 11; **(author?)** 12; **(author?)** 13; **(author?)** 14; **(author?)** 15) and against (**(author?)** 8; **(author?)** 16) mergers, disk instabilities (**(author?)** 17; **(author?)** 18), nuclear supernovae (**(author?)** 19; **(author?)** 20), disk instabilities caused by supernovae [21], starbursts [22], stellar collisions (**(author?)** 23; **(author?)** 24) and gravitational microlensing [25].

Nonetheless, we are currently unable to observe any given galaxy and know with certainty how and why it is has been, or will become, active in it's lifetime. Current statistics can be based only on observations which "catch" galaxies in their active phase and these studies have found AGN activity to peak at $z \approx 2$ or *"cosmic noon"*. It also finds a stunning connection between the abundance of AGN in a given epoch and cosmic star formation rates, with the two processes largely tracing each other [26]. However this assumes current selection methods finds a complete sample of active galaxies within the universe.

Luckily, AGN emission is not static and actually varies in flux over time in every wavelength it has been observed in [27] and we can take advantage of this to study them.

Variability studies are a powerful tool in analysing AGN activity as they rely on the change in flux in a given wavelength (or wavelengths) and therefore does not require high quality imaging to work. In addition to this variabil-

ity observations are attributed to stochastic processes within the AGN itself, and this allows for the study of AGN on the relatively tiny scales they span compared to the radial size of a galaxy. This advantage extends to obscured galaxies as well as high redshift, where the AGN would be unresolvable.

One caveat, however, is that variability timescales increase with wavelength, with higher frequencies such as X-rays varying on second to minute timescales, UV and optical taking days to weeks and the longer wavelengths, such as the infrared (IR), requiring months or even years for significant variability to be seen [18]. These wavelengths also couple to structures within the AGN, as longer wavelengths link to longer distances from the core. X-rays, for example, are generated in the X-ray corona with UV and optical photons being emitted from the accretion disk and infrared emission originating in the surrounding dusty torus.

Though IR observations present a unique opportunity to study the hottest part of the dusty torus as it falls into the accretion disk, this is far less well studied compared to smaller scales due to the time and resources required for IR variability to be observed.

This can be seen from previous works, with research focusing on a handful or individual objects (**(author?)** 28, **(author?)** 29, **(author?)** 30), otherwise selecting AGN by other means (**(author?)** 31, **(author?)** 27, **(author?)** 32), studying them via IR light curves that are not well sampled [33] or are constructed from multiple different surveys and observations [34].

In this research we make use of nearly a decade of IR observations the Ultra Deep Survey was the first to provide to select active galaxies based purely on their IR variability using the technique developed in **(author?)** 35. We then compare the properties and environment of these active galaxies found using near-infrared variability to active galaxies found using X-ray emission and regular, inactive galaxies to determine any similarities or differences. This allows us to identify possible triggering mechanisms for AGN activity as well as see how the incidence of this activity changes over cosmic time.

The layout of this paper is as follows. In section **??** we describe the data sets used for this research and in section **??** we describe the methodology used to select and study the active galaxies. Section **??** contains our results and finally section **??** contains a summary of the research, the conclusions we draw from our analysis and a brief mention of future work.

All magnitudes stated are AB magnitudes and we use a Λ cold dark matter (ΛCDM) cosmology, with $H_0 = 70 kms^{-1}Mpc^{-1}$, $\Omega_\Lambda = 0.7$ and $\Omega_m = 0.3$.

Chapter 2

Data

2.0.1 Summary of surveys

In this research we make use of multiple deep surveys. The United Kingdom Infrared deep sky survey (UKIDSS), Ultra Deep Survey (UDS) 11^{th} data release (Almaini et al., in prep), The Chandra Legacy Survey of the Ultra Deep Field ([36]) as well as morphological and environmental measurements of the field. The first provides the data necessary to select active galaxies based on their IR variability, and the second provides access to a complimentary set of X-ray bright active galaxies and we use radio imaging to classify the AGN into radio quiet and radio loud.

We also made use the 1.4GHz radio imaging described in [37], taken using The Very Large Array, and found that all of the active galaxies in this sample are radio quiet.

2.0.2 UDS DR11

The United Kingdom Infrared Telescope (UKIRT) Infrared Deep Sky Survey (UKIDSS) Ultra Deep Survey (UDS), referred to from now on as the UDS, is the deepest survey over $\sim 1 deg^2$. It has 296,007 sources, covers 12 bands in the optical and IR (U, B, V, R, i', z', Y, J, H, K, 3.6, 4.5), has an 8 year baseline for IR observations and a 5σ point-source limiting depth of J = 25.6

and K = 25.3 AB mag in 2 arcsec diameter apertures (Almaini et al., in prep). Version 11 is the latest data release of the Ultra Deep Survey (UDS DR11). From this we make use of the "best galaxies" subset which contains objects identified in unmasked regions of the field, have reliable photometry in all 12 bands, have the deepest IRAC imaging and have cross-talk and candidate stars removed. This leaves 202,282 sources remaining for analysis.

2.0.3 Redshift

Where available spectroscopic redshifts are used, otherwise photometric redshifts are used in all cases except for the IR variable AGN.

For the non variable objects, photometric redshifts were calculated according to the methodology described in [38], where the 12 available bands of photometry were fit with stellar synthesis models provided by [39] using the publicly available code EAZY ([40]). These redshifts have a typical accuracy of $\frac{\Delta z}{(1+z)} \approx 0.018$ and other properties, such as mass and luminosity were based on them (Almaini et al., in prep).

Due to the variable nature of the IR variable active galaxies, photometric redshifts were recalculated, again using the EAZY redshift code, but with an additional reddened and un-reddened AGN templates. This produced the final redshifts used for the variable AGN throughout this research.

2.0.4 Chandra X-ray catalogue

The UDS field has deep Chandra X-ray imaging of a fraction of the field. This were carried out using The Chandra Space Telescope's Advanced CCD Imaging Spectrometer, covering $0.33deg^2$ in total, the central $100arcmin^2$ of which overlaps with UDS imaging ([36]). It has a flux limit of $4.4x10^{-16}ergs^{-1}cm^{-2}$ in the full band $(0.5 - 10keV)$ and identifies 868 sources in total. Matching to the UDS DR11 on RA and Dec within 1" provides a sample of 710 X-ray bright active galaxies for use in this study, 107 of which are also classed as IR

variable active galaxies (section 3.0.1).

2.0.5 Merger features

Classifications of morphology and recent merger features is provided by [41] as part of the citizen science collaboration 'Galaxy Zoo'. Here expert participants classified the visual morphologies of galaxies using imaging from The Cosmic Assembly Near-infrared Deep Sky Survey, Ultra Deep Survey (CANDELS UDS), which is a spaced based optical and IR survey, based on The Hubble Space Telescope, which has imaged part of the wider UDS field.
Recent mergers and interactions are defined as objects that show signs of tidal debris and/or multiple merging cores.

2.0.6 Environment

Environmental number densities for galaxies within the UDS are calculated using the technique described in [42]. For each galaxy a cylindrical volume was constructed based on a 250kPC radius and ±0.5GYr "height". Within this volume the number of neighbouring galaxies were counted, this value was then normalised according to both the area of unmasked pixels within that volume (to account for holes and/or edges within the field) as well as the total number of galaxies within the considered volume, to give the value of density. This number density, ρ_{250}, is environmental density measure we make use of in this analysis.

Chapter 3

Method

3.0.1 Selecting AGN based on their IR variability

Infrared variable AGN were selected from the UDS DR11 using the technique first developed and used in [35]. From the 114,243 light curves available, a sample of 705 active galaxies were identified for study. A vast majority of these are newly discovered, as only ∼37% of the IR variable active galaxies are found in deep X-ray surveys when we compare the active galaxies identified in the shared UDS and Chandra imaging region (107/292).

Light curves for the galaxies were constructed from multiple flux measurements. This spanned 8 semesters in the J-band and 7 semesters in the K-band (one K-band semester did not have enough observations to be included). AGN were then selected using a χ^2 analysis, as seen in equation 3.1, based on the assumption that a vast majority of galaxies in the universe are intrinsically non-variable.

In order to ensure differences in flux measurements were due to intrinsic AGN variability and not changes in the point spread function from semester to semester, each semester stack of images was convolved with a Gaussian kernel to match the stack with the poorest quality PSF. A preliminary χ^2 analysis was then performed to remove the most variable sources and the light curves were normalised, and split into bins based on flux, epoch and quadrant. From this

the standard deviation of the grouped flux values provided the photometric error on the measurements ([35]).

$$\chi^2 = \sum_i \frac{(F_i - \bar{F})^2}{\sigma_i^2} \tag{3.1}$$

Finally we define our χ^2 as is shown in equation 3.1 were F_i is the flux of an object, σ_i is the corresponding uncertainty and $\bar{F}$ is the mean flux of that object across all imaging epochs. A threshold of $\chi^2 > 30$ was used for the K-band and $\chi^2 > 32.08$ for the J-band which gives the same P-value for both χ^2 distributions accounting for the different number of imaging epochs and therefore differing degrees of freedom.

3.0.2 Galaxies on the edge of the science image

Visual inspection found that a sample of galaxies on the edge of the science image were classified as hosting variable AGN. To investigate if these objects were real, we took the time to isolate them and look at their images individually in each epoch to determine their validity. Of the 104 identified edge cases, clear issues with $\sim 33\%$ of them was found, however we were unable to identify if there was a systematic problem that explained why these particular cases were classed as hosting AGN. As such, we re-ran all analysis both with and without this sample of galaxies, and found no significant change in the overall trends. Therefore, we decided to remove these objects entirely from the analysis to ensure our results are robust. The remaining sample consists of 601 galaxies.

3.0.3 Measuring real variability: Maximum Likelihood

For any measurement of an active galaxy light curve we know that observed changes in flux are due to a combination of the intrinsic magnitude variations due to the active galactic nuclei (σ_Q), and noise (σ_{noise}). If we are to measure the properties of the AGN, we have to be able to separate out these two effects.

$$\sigma_{obs} = \sigma_Q + \sigma_{noise} \tag{3.2}$$

As such, to calculate the variability amplitude of a given AGN (σ_Q) we make use of a maximum likelihood technique. This technique, developed in [43], allows for the measurement of the noise subtracted, intrinsic variance of the AGN within a given active galaxy and is given in equation 3.3.

$$L(\sigma_Q|x_i\sigma_i) = \prod_{i=1}^{N} \frac{e^{\frac{-(x_i-\bar{x})^2}{2(\sigma_i^2+\sigma_q^2)}}}{(2\pi)^{1/2}(\sigma_i^2+\sigma_Q^2)^{1/2}} \tag{3.3}$$

To begin we normalise each light curve such that the average flux ($\bar{x}$) is equal to 1. Then, using the value of the flux in each bin (x_i) and its corresponding measurement error (σ_i) we calculate the likelihood function, $L(\sigma_Q|x_i\sigma_i)$ for 1001 equally spaced values of possible AGN variability amplitudes between 0 and 1 inclusive. From this we generate a likelihood curve.

Then to determine σ_Q for each active galaxy, we simply select the value of σ_Q that maximises the likelihood function. 1σ errors are calculated by assuming a Gaussian fit to the curve. An example can be seen in Figure 3.1.

3.0.4 Simulating variability

The maximum likelihood technique described in section 3.0.3 calculates a noise subtracted value for the AGN variability amplitude and is therefore extremely sensitive to the errors on a given flux measurement. A major barrier in being able to compare all of the galaxies in the sample equally is due to their redshift and therefore apparent magnitude, as objects that are at higher redshifts and/or are intrinsically dimmer, will have systematically larger uncertainties on their measurements.

To be able to take advantage of the excellent, near decade of imaging and wide redshift range provided by the UDS, we calculate variability amplitude confidence detection curves for the brightness range of our sample.

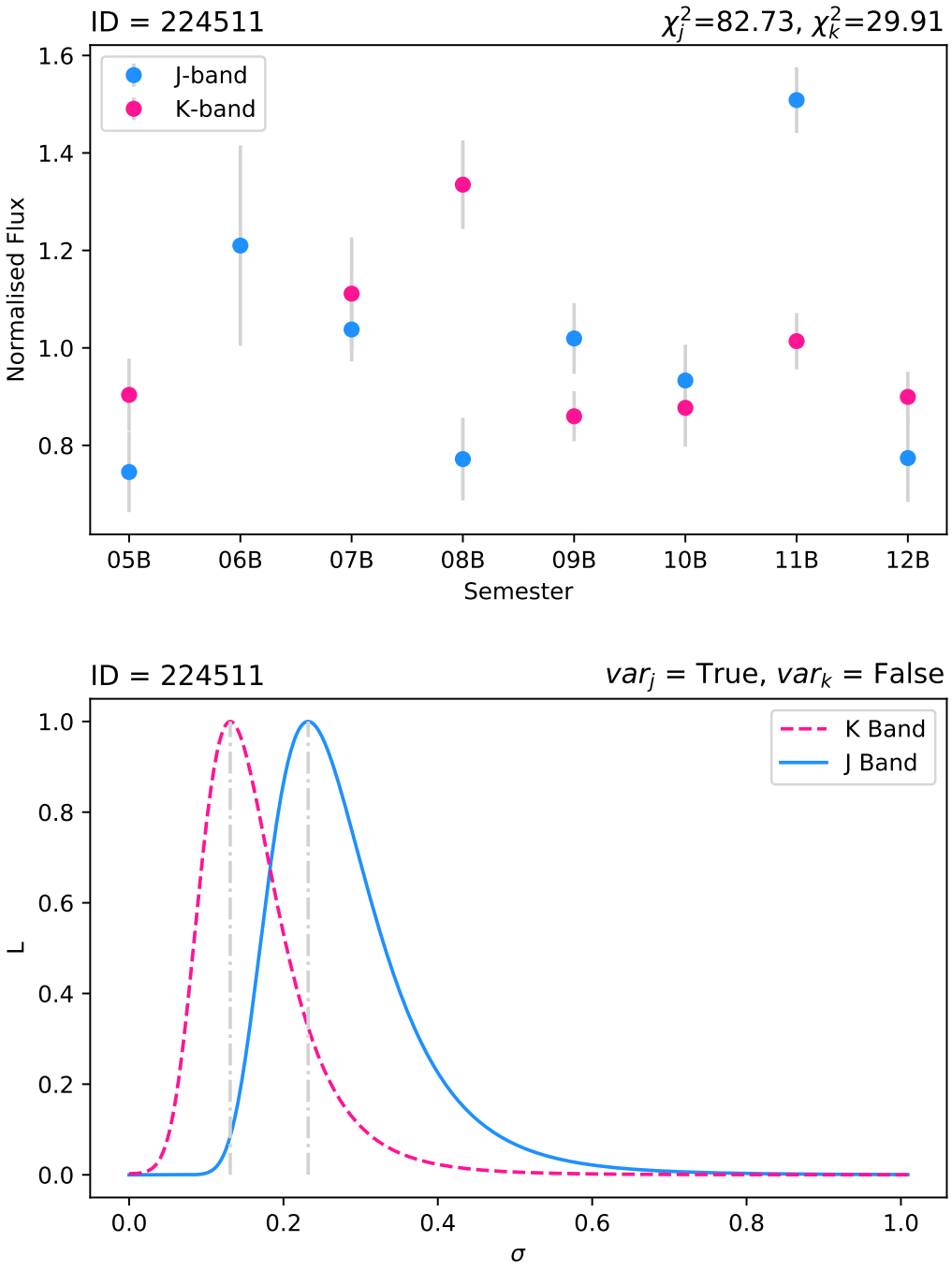

Figure 3.1: *Example of an active galaxy light curve (left) and corresponding normalised likelihood curve (right). The threshold for recovery of AGN variability from a given light curve is χ^2_K ¿ 30 and χ^2_J ¿ 32.08 in the K and J bands respectively. As shown by the grey lines in the right plot the AGN variability amplitude is determined by selecting the corresponding value for σ_Q that maximises the likelihood function. This galaxy is only classified as variable in the J-band (blue), as shown by the value of the χ^2.*

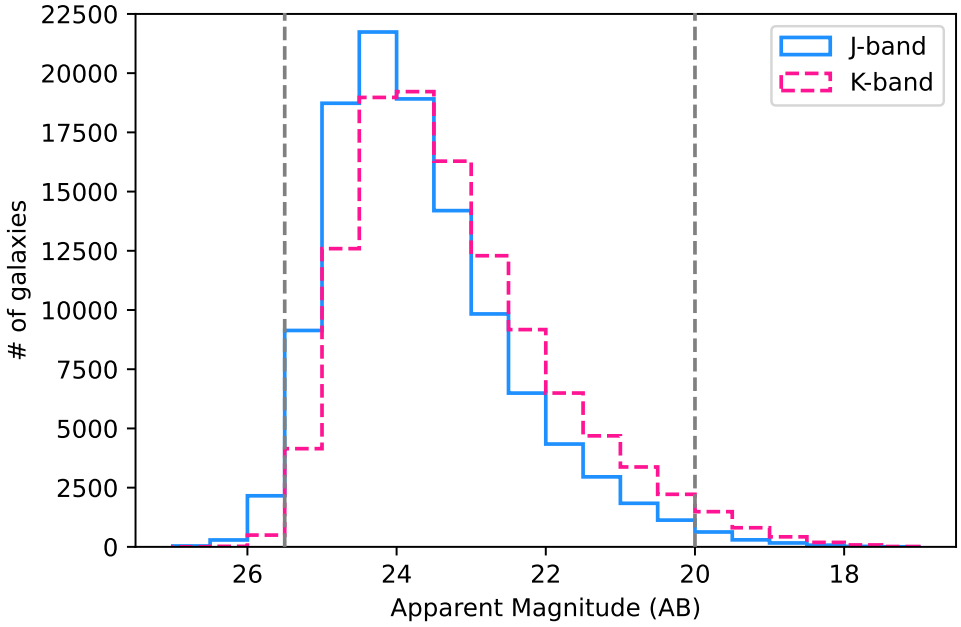

Figure 3.2: *Distribution of apparent magnitude for 112,979 regular, inactive galaxies. Blue solid lines represents the J-band apparent magnitude, red dashed lines shows the K-band. The x-axis has been reversed to reflect the fact that brighter objects have smaller magnitudes. Vertical grey dashed lines denote the extremes of the distribution beyond which the remaining high and low magnitude ends have been grouped together. Excluding the extremes, each bin is* $\Delta m = 0.5$ *in width.*

To begin, we remove *any* active galaxy from our initial sample of 114,243 galaxies and then split what remains (inactive/regular galaxies) into bins based on apparent magnitude (Fig 3.2).

Then to simulate variability in these galaxies we, generate a Gaussian distribution of values. Each Gaussian distribution has a mean of 0 and a standard deviation that can be 101 values between 0 and 1 inclusive. We then add each version of values in turn to the flux measurements within the regular galaxy light curve. Finally, we take our new light curve, with simulated variability, and run the χ^2 and maximum likelihood analysis on it. This allows us to test three things:

1. The minimum variability amplitude that is detectable in each flux bin.

2. The minimum variability amplitude required for an AGN to be detectable for a given flux.

3. To compare how close the amplitude recovered is to the amplitude we put in, and how this changes with flux.

After comparing the recovered artificial AGN variability amplitude to the value input, we calculated the Pearson rank correlation coefficient (ρ_r) for each flux bin. Using this we find that the maximum likelihood technique works extremely well for all bins, with the lowest correlation being $\rho_r = 0.86$. This was found the the dimmest J-band bin and had a corresponding P-value of $p_r = 10^{-30.7}$.

3.0.5 Variability detection limit

Now that we are satisfied with the effectiveness of the likelihood technique, we use it to calculate the flux dependant minimum detectable variability. For each value of artificial variability (σ_Q) added to the galaxies, we calculate a χ^2, classify the galaxy as hosting an AGN or not based on this value and the limit developed in [35], and use the results to determine the fraction of galaxies now considered to be active in that flux bin (Fig: 3.3).

Reading off the values for σ_Q for different fractions of galaxies we are able to generate multiple detection limit confidence curves for our entire brightness range. As seen in figure 3.5, given the apparent magnitude and variability amplitude of a variable active galaxy, we are able to determine how likely it is the measured variability amplitude is real. Throughout this research we make use of the 90% threshold as this was found to be the highest confidence level that retained a significant amount of galaxies for analysis. Further to this we chose to use the J-band detection curve over the K-band detection curve as figure 3.3 shows that higher amplitudes are required in the J-band imaging for variability to be detected. This minimises the chance of false detections.

All analysis was done both with and without this filtering, and the overall trends we report in section **??** do not change significantly, showing our results are robust. Results presented in this paper are filtered via the detection limit

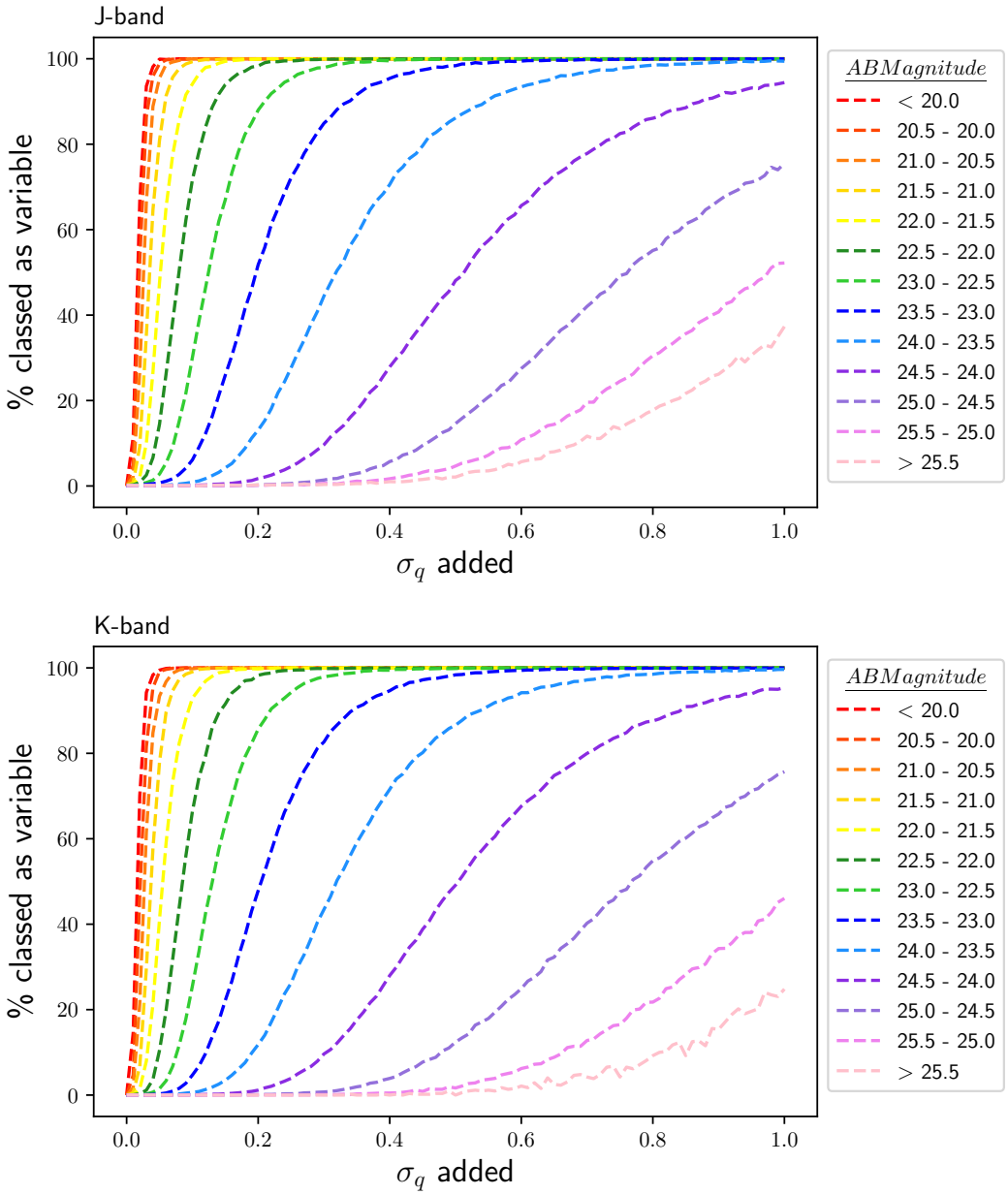

Figure 3.3: *Curves showing the fraction of galaxies classed as hosting variable AGN compared to the level of artificial variability added for J-band (left) and K-band (right) imaging of inactive galaxies. Each dashed line represents a different apparent magnitude bin. In the brightest bins, lower uncertainties on measurements allow for small amounts of variations to be recoverable. However, significant amounts of variability is required for AGN to be detected in the dimmest galaxies.*

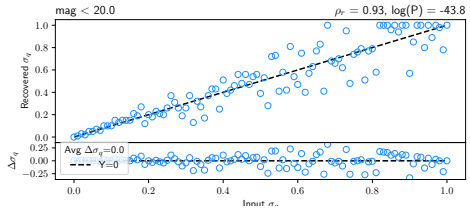
mag < 20.0
ρ_r = 0.93, log(P) = -43.8
Recovered σ_q
$\Delta\sigma_q$
Avg $\Delta\sigma_q$=-0.0
Y=0
Input σ_q

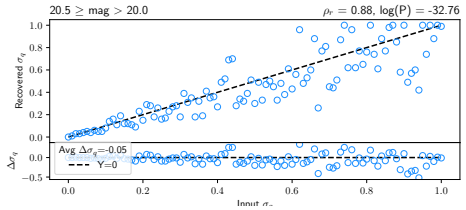
20.5 ≥ mag > 20.0
ρ_r = 0.88, log(P) = -32.76
Recovered σ_q
$\Delta\sigma_q$
Avg $\Delta\sigma_q$=-0.05
Y=0
Input σ_q

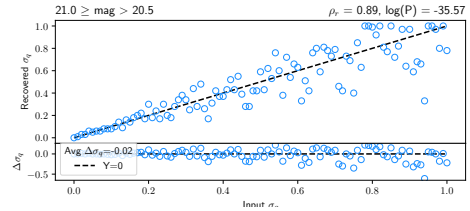
21.0 ≥ mag > 20.5
ρ_r = 0.89, log(P) = -35.57
Recovered σ_q
$\Delta\sigma_q$
Avg $\Delta\sigma_q$=-0.02
Y=0
Input σ_q

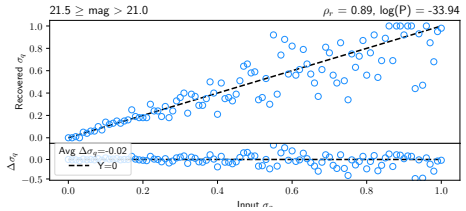
21.5 ≥ mag > 21.0
ρ_r = 0.89, log(P) = -33.94
Recovered σ_q
$\Delta\sigma_q$
Avg $\Delta\sigma_q$=-0.02
Y=0
Input σ_q

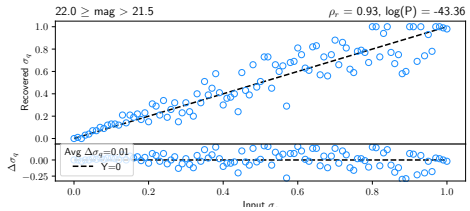
22.0 ≥ mag > 21.5
ρ_r = 0.93, log(P) = -43.36
Recovered σ_q
$\Delta\sigma_q$
Avg $\Delta\sigma_q$=0.01
Y=0
Input σ_q

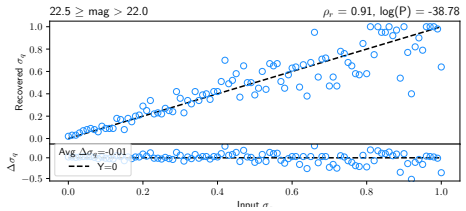
22.5 ≥ mag > 22.0
ρ_r = 0.91, log(P) = -38.78
Recovered σ_q
$\Delta\sigma_q$
Avg $\Delta\sigma_q$=-0.01
Y=0
Input σ_q

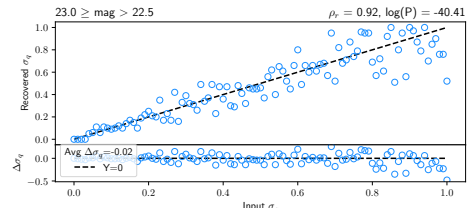
23.0 ≥ mag > 22.5
ρ_r = 0.92, log(P) = -40.41
Recovered σ_q
$\Delta\sigma_q$
Avg $\Delta\sigma_q$=-0.02
Y=0
Input σ_q

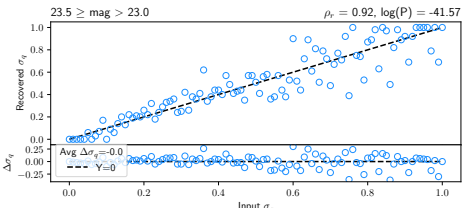
23.5 ≥ mag > 23.0
ρ_r = 0.92, log(P) = -41.57
Recovered σ_q
$\Delta\sigma_q$
Avg $\Delta\sigma_q$=-0.0
Y=0
Input σ_q

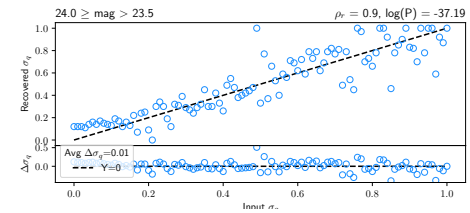
24.0 ≥ mag > 23.5
ρ_r = 0.9, log(P) = -37.19
Recovered σ_q
$\Delta\sigma_q$
Avg $\Delta\sigma_q$=0.01
Y=0
Input σ_q

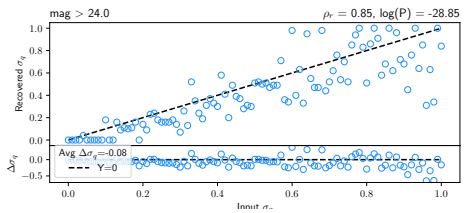
mag > 24.0
ρ_r = 0.85, log(P) = -28.85
Recovered σ_q
$\Delta\sigma_q$
Avg $\Delta\sigma_q$=-0.08
Y=0
Input σ_q

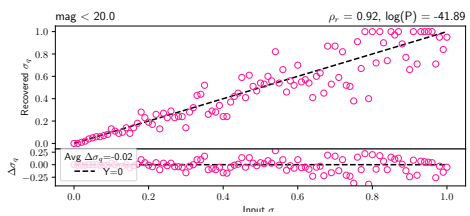
mag < 20.0
ρ_r = 0.92, log(P) = -41.89
Recovered σ_q
$\Delta\sigma_q$
Avg $\Delta\sigma_q$=-0.02
Y=0
Input σ_q

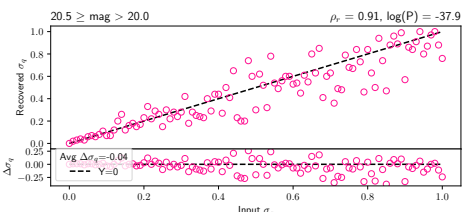
20.5 ≥ mag > 20.0
ρ_r = 0.91, log(P) = -37.9
Recovered σ_q
$\Delta\sigma_q$
Avg $\Delta\sigma_q$=-0.04
Y=0
Input σ_q

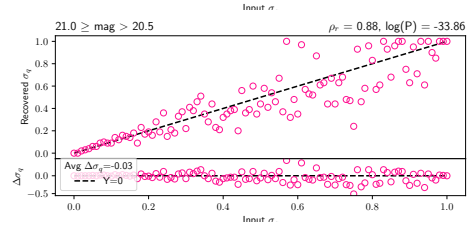
21.0 ≥ mag > 20.5
ρ_r = 0.88, log(P) = -33.86
Recovered σ_q
$\Delta\sigma_q$
Avg $\Delta\sigma_q$=-0.03
Y=0
Input σ_q

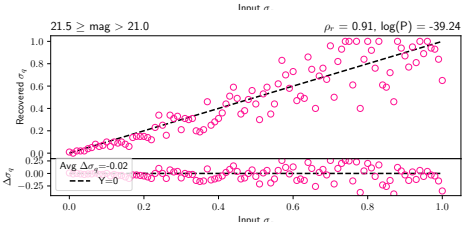
21.5 ≥ mag > 21.0
ρ_r = 0.91, log(P) = -39.24
Recovered σ_q
$\Delta\sigma_q$
Avg $\Delta\sigma_q$=-0.02
Y=0
Input σ_q

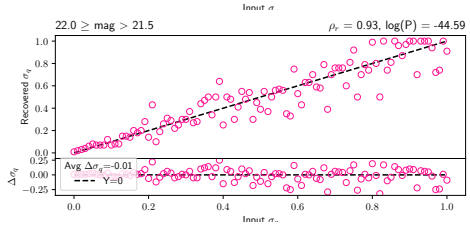
22.0 ≥ mag > 21.5
ρ_r = 0.93, log(P) = -44.59
Recovered σ_q
$\Delta\sigma_q$
Avg $\Delta\sigma_q$=-0.01
Y=0
Input σ_q

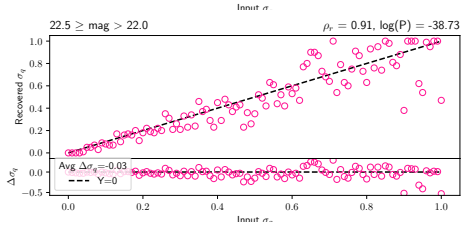
22.5 ≥ mag > 22.0
ρ_r = 0.91, log(P) = -38.73
Recovered σ_q
$\Delta\sigma_q$
Avg $\Delta\sigma_q$=-0.03
Y=0
Input σ_q

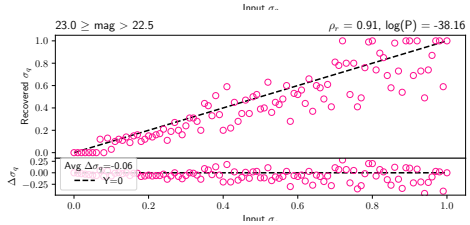
23.0 ≥ mag > 22.5
ρ_r = 0.91, log(P) = -38.16
Recovered σ_q
$\Delta\sigma_q$
Avg $\Delta\sigma_q$=-0.06
Y=0
Input σ_q

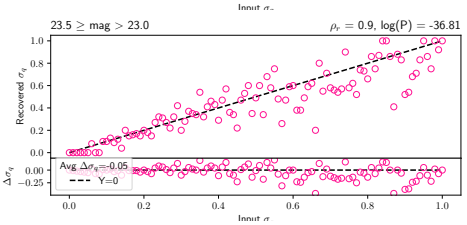
23.5 ≥ mag > 23.0
ρ_r = 0.9, log(P) = -36.81
Recovered σ_q
$\Delta\sigma_q$
Avg $\Delta\sigma_q$=-0.05
Y=0
Input σ_q

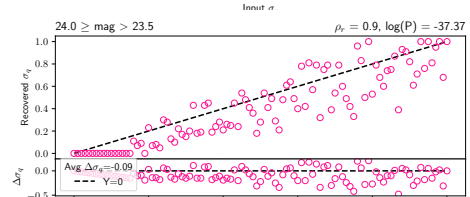
24.0 ≥ mag > 23.5
ρ_r = 0.9, log(P) = -37.37
Recovered σ_q
$\Delta\sigma_q$
Avg $\Delta\sigma_q$=-0.09
Y=0
Input σ_q

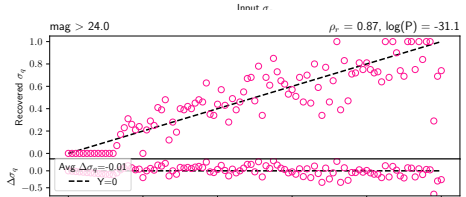
mag > 24.0
ρ_r = 0.87, log(P) = -31.1
Recovered σ_q
$\Delta\sigma_q$
Avg $\Delta\sigma_q$=-0.01
Y=0
Input σ_q

curves.

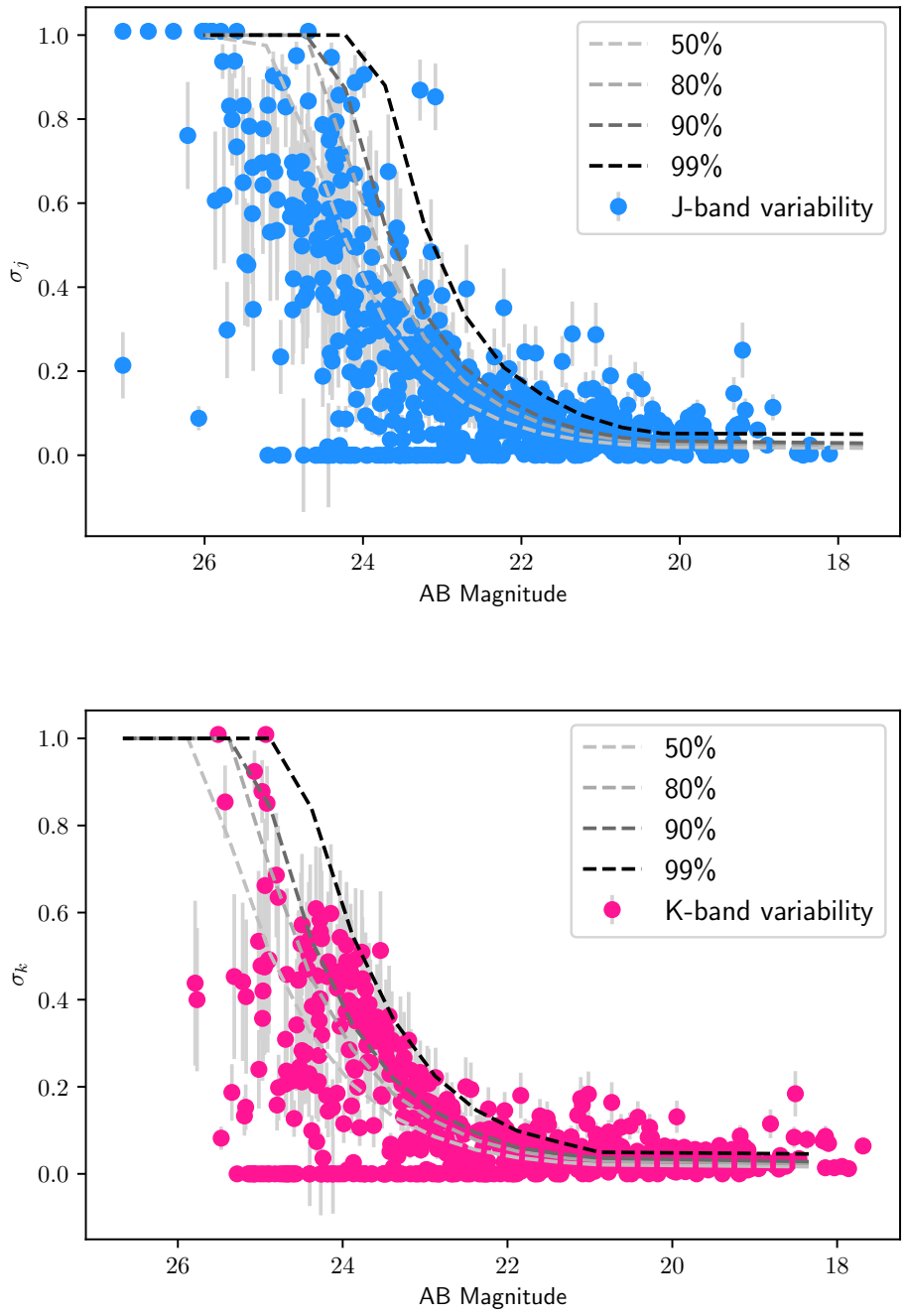

Figure 3.5: *AB magnitude vs variability amplitude for the real variable active galaxies. Blue points indicate galaxies selected as hosting variable AGN in the J-band, pink points show the same but for the K-band. Grey 1σ errors are based on assuming a Gaussian fit to the likelihood curves. Overlaid are detection limit curves for different levels of certainty. Throughout this research we use the 90% curve as this provides the highest level of certainty without over-reducing the sample.*

Chapter 4

Variable AGN vs X-ray AGN

4.1 Results

4.1.1 A new type of Active Galaxy

We first find that this detection method is successful in identifying AGN activity in galaxies previously thought to be quiescent. When limiting both surveys to the same area of sky, the samples are largely separated, with the percentage of dual detected AGN (these are X-ray bright AGN that are are variable in the NIR) being only ≈37% (107/292).

Further evidence supporting the hypothesis that IR variability selects a more diverse range of active galaxies compared to X-ray selection methods can be seen by examining the stellar masses. Figure 4.1 shows that there is a clear distinction in the mass ranges between the X-ray and variability selected active galaxies, with variable AGN residing in galaxies with a wider range of masses compared to X-ray AGN which primarily probes higher mass galaxies.

We also rule out the possibility that these new, variable AGN are X-ray AGN that are too dim for their X-ray emission to be observed using current instrumentation. In figure 4.2 we plot the ratio of the 2keV X-ray luminosity to the rest frame optical luminosity at 2500Å for the sample, using upper limits for non-X-ray detected objects. Here we find that the variable active galaxies have

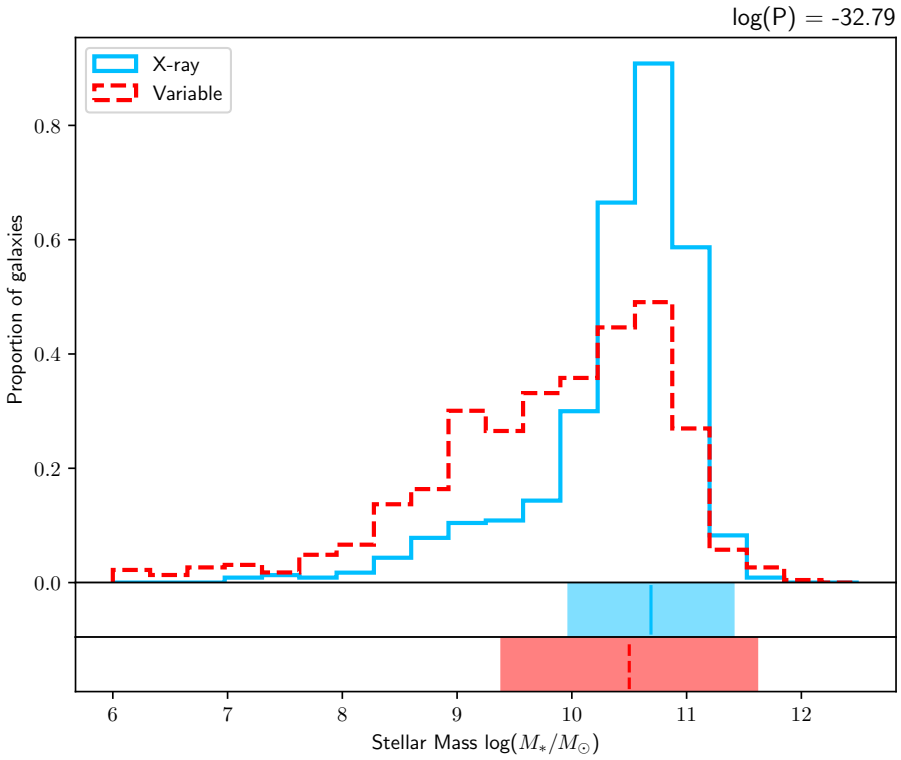

Figure 4.1: *Normalised histograms showing the distribution in stellar mass of active galaxies in our sample. Galaxies are separated according to detection method, where the blue solid-lined histogram represents X-ray selected active galaxies, and the red dashed histogram shows objects classified as hosting variable AGN. Corresponding coloured distributions below the histograms show the average and 1σ standard deviation. The P-value comes from a Kolmogorov-Smirnov (KS) test which confirms that samples are probing different underlying distributions.*

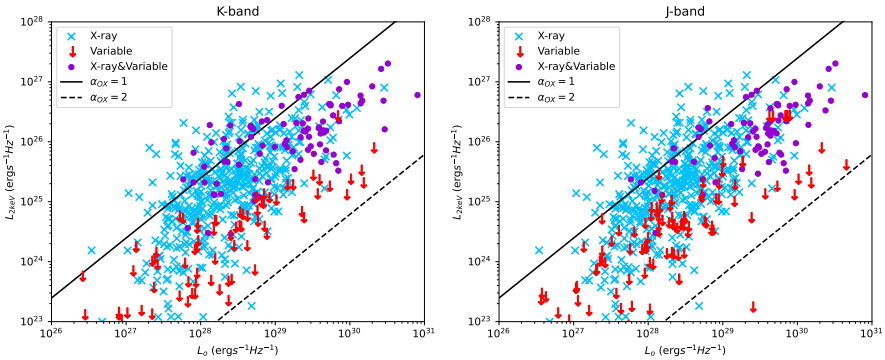

Figure 4.2: *Monochromatic 2keV X-ray luminosity vs rest-frame optical luminosity at 2500Å for objects imaged within the Chandra region of the UDS field. X-ray bright active galaxies are denoted by blue crosses and AGN detected by both NIR variability and X-ray emission are highlighted as purple dots. Upper limits are used for variability detected active galaxies without X-ray detections, and are shown by red arrows. Black lines indicate the slopes corresponding to a spectral index of α_{ox}=1 (solid) and α_{ox}=2 (dashed) in the rest frame.*

similar optical luminosities compared to X-ray bright active galaxies, but are systematically more X-ray quiet. This is further strengthened by dual detected objects having X-ray luminosities expected of truly X-ray bright objects. This shows that variability finds a new set of AGN in galaxies are otherwise missed by X-ray scans of the sky.

Comparison of measured structural parameters finds further differences in the samples. In figures 4.3 and 4.4 we compare the galactic morphologies and radial sizes respectively. Here we find variable AGN hosts skew more disk-like in shape and are smaller in size compared to X-ray bright active galaxies, features which are consistent with what one would expect when comparing low mass galaxies to high mass galaxies.

Overall, comparison of the structural properties shows that AGN activity has seemingly no preference for the type of galaxy it exists in, with different detection methods identifying the black hole accretion process in intrinsically distinct galaxy types.

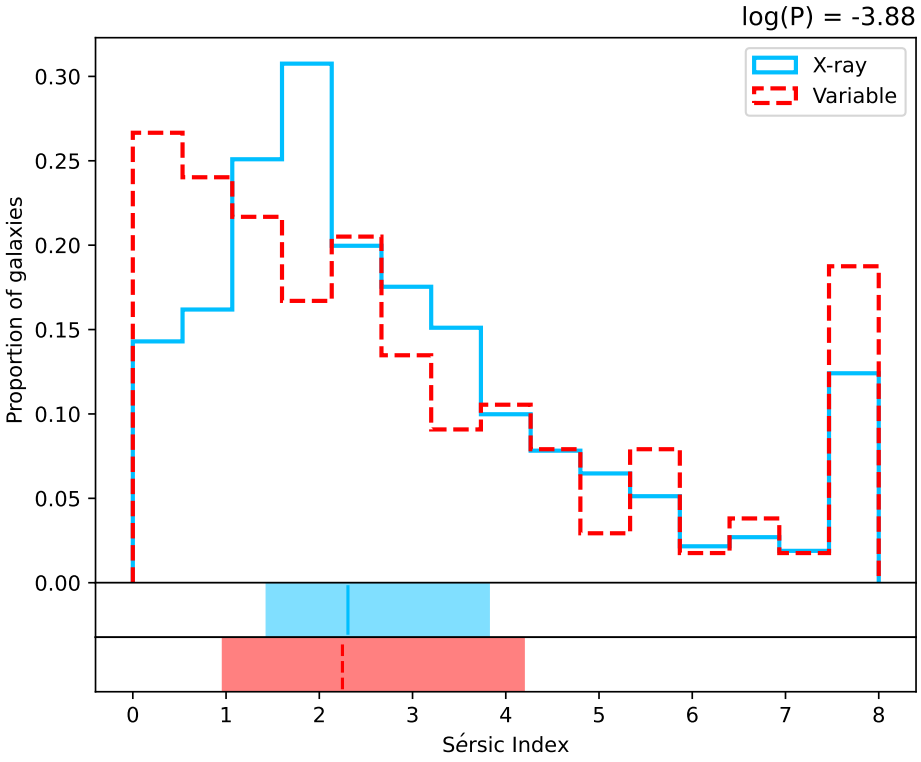

Figure 4.3: *Normalised histogram of measured Sérsic index of active galaxies. Blue solid lines represents X-ray detected active galaxies and red dashed lines represents variability detected active galaxies. Colour matched distributions below the histograms show the median value and interquartile range. The P-value arises from a KS test between the two distributions.*

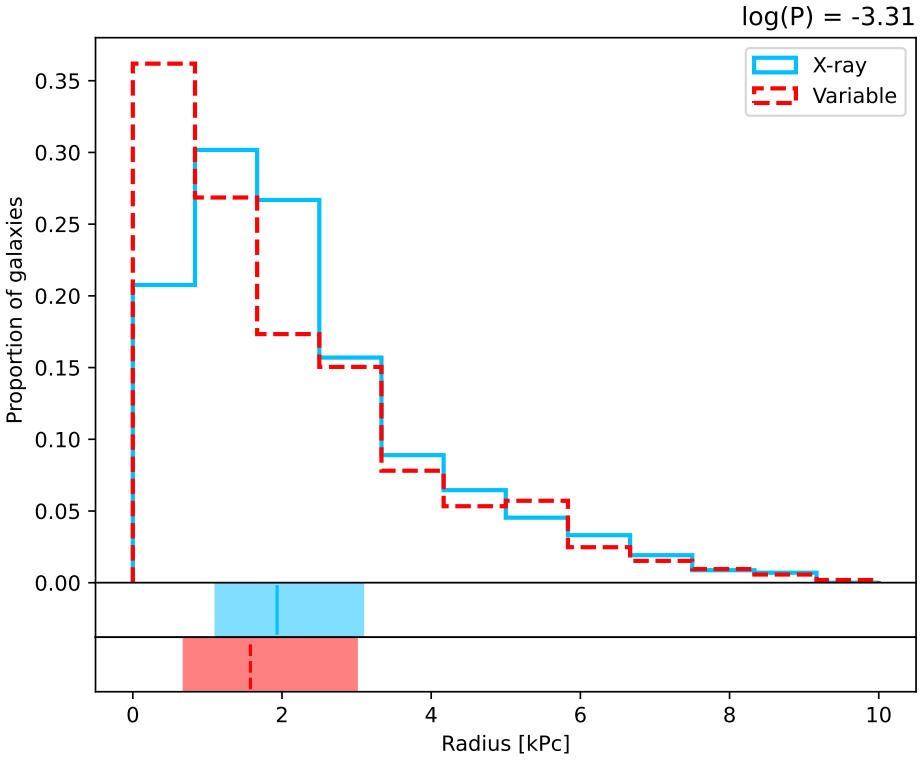

Figure 4.4: *Normalised histogram of the active galaxies' radius, given in kPc. Blue solid lines represents X-ray detected active galaxies, red dashed lines represents variability detected active galaxies. Colour matched distributions below histograms show the median value and interquartile range. Reported P-value is from a KS test and finds that the active galaxies are sampling different underlying distributions.*

4.1.2 AGN fraction over cosmic time

Another aspect of this investigation is to explore the question: how does the fraction of AGN in the universe change over cosmic time? Previous studies find that AGN activity is much less common now than it was earlier in the universe, with activity peaking around *'cosmic noon'* (z≈2) and tracing cosmic star formation rates at all redshifts (see [44], figure 15). This is generally attributed to the larger abundance of gas available for accretion onto a black holes in the early universe, however as shown in section 4.1.1, NIR variability does not require high mass, high luminosity galaxies or high quality imaging to identify AGN activity and does find activity in galaxies previously thought to be dormant, making it an excellent method to trace black hole accretion in the distant universe.

To accurately answer this question we must be able to compare the galaxies in the sample in a fair and equal way. For any observation of the night sky only the brightest objects will be viewable at high redshift. In addition to this, as reported in figure 4.1 the active galaxies in this sample probe significantly different mass ranges, so for a reasonable comparison to be made we first take a mass cut in the data to ensure a consistent range across all of the redshifts being considered.

This results in us requiring all galaxies in this section of analysis to have a stellar mass of $\log(M_*/M_\odot) \geq 10$, figure 4.5 illustrates the galaxy selection.

Now that the sample is consistent in mass, we turn our attention to the variable sample. To ensure the variability amplitudes we consider across all wavelengths are trustworthy, we make use of the detection curves calculated in section 3.0.5. We find that using the 90% confidence curve gives the best compromise between the highest certainty on the measurement without over-reducing the sample. Here we select a limit where we can trust measured variability amplitudes down to the 20% level. We make use of the J-band curve over the K-band curve as for a given variability amplitude and confidence level, the

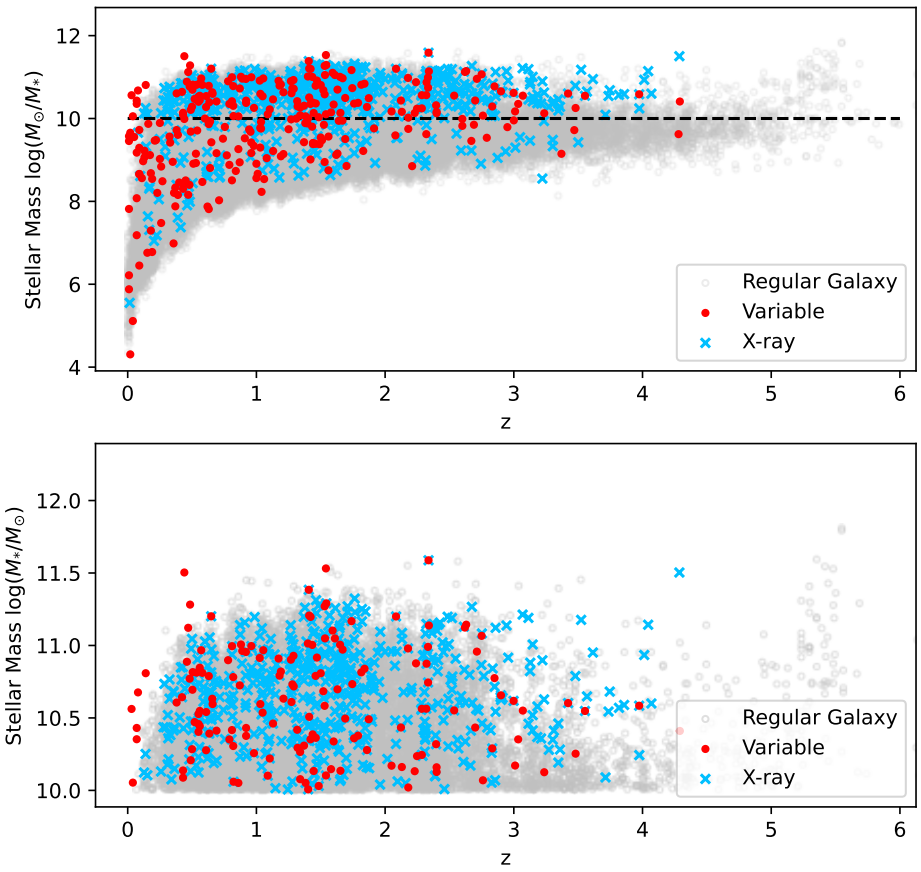

Figure 4.5: *Top: Stellar mass - redshift distribution for all galaxies in the data. Bottom: Stellar mass - redshift distribution for galaxies with stellar mass* $\log(M_*/M_\odot) \geq 10$. *Blue crosses represent X-ray detected active galaxies, red dots show variable active galaxies. Grey open circles represent regular inactive galaxies. Horizontal black dashed line in the top plot shows the* $\log(M_*/M_\odot) \geq 10$ *mass limit.*

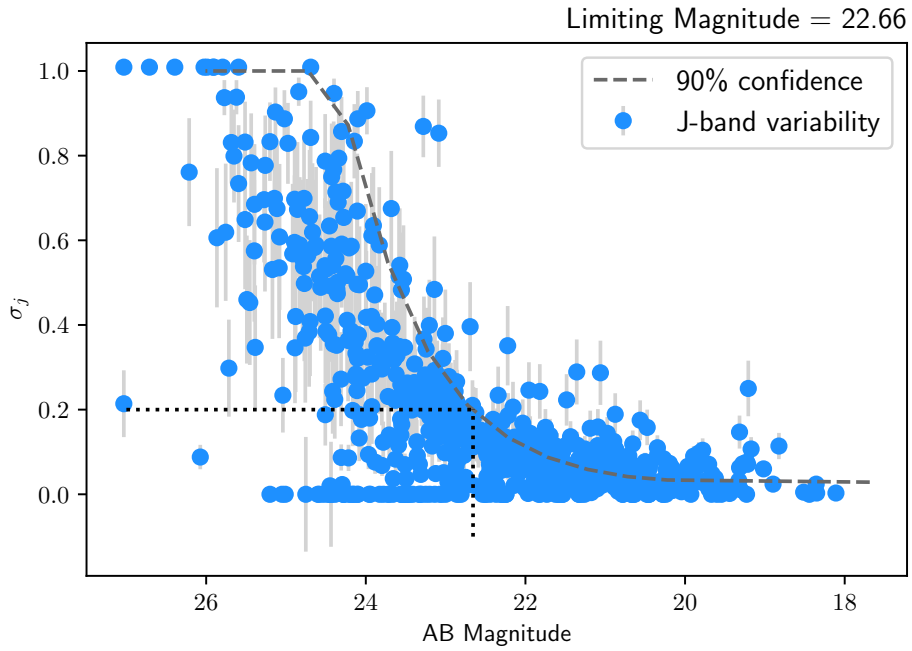

Figure 4.6: *J-band variability amplitude vs AB magnitude for variable AGN in the sample. Blue dots are measured amplitudes with 1σ errors based on a Gaussian fit to the likelihood curve. Dashed grey line is the 90% confidence curve calculated from simulating variability in regular, inactive galaxies. Dotted black line illustrates how an apparent magnitude limit of $m_J \leq 22.66$ is required to trust variability measurements down to the 20% level.*

J-band requires brighter galaxies. Figure 4.6 illustrates how we use the confidence curve to obtain the maximum magnitude of $m_J \leq 22.66$, beyond which we consider galaxies to be too dim for their measured variability amplitude to be trusted in this section of analysis.

Applying this to the mass matched galaxies (see figure 4.5, bottom) leaves us with the final group to be studied (figure 4.7).

To calculate the fraction of active galaxies within a given epoch, we take the samples and bin them according to redshift.

Using a bin width of $\Delta z = 0.5$ we produced figure 4.8, which shows how the fraction of active galaxies in the universe peaks as $z \approx 3$. A KS-test does not find the AGN fractions to be sampling different underlying distributions. Two main results come from this. The first is that we find AGN activity to peak very early in the universe, prior to the peak of star formation at $z = 2$. In addition to this, this early maximum activity occurs for all active galaxies in

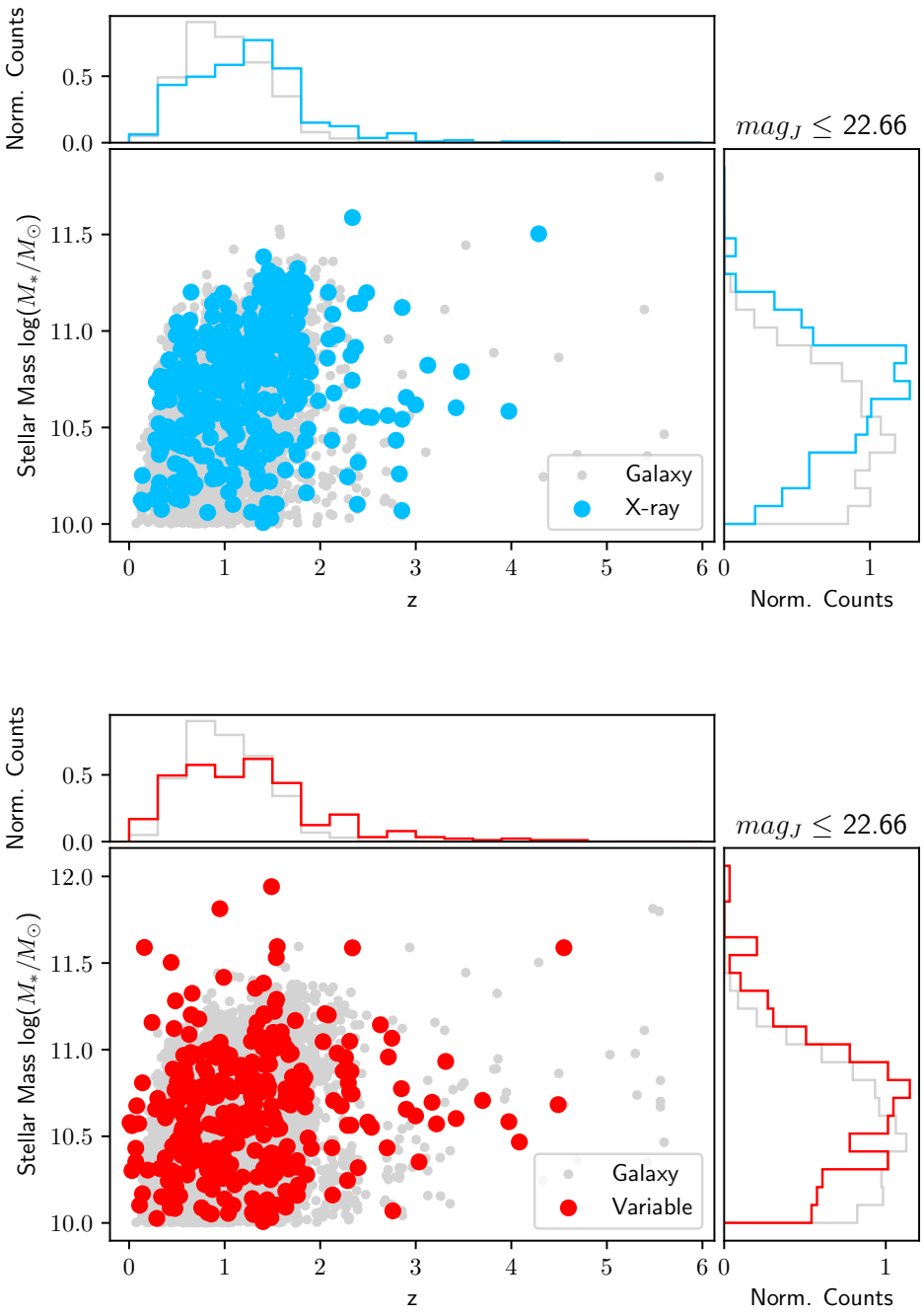

Figure 4.7: *Stellar mass - redshift distribution for galaxies with $log(M_*/M_\odot) \geq 10$ and $m_J \leq 22.66$. X-ray bright active galaxies are shown in blue, variability selected active galaxies are shown in red and the comparative sample of galaxies are shown in grey. For the X-ray sample all galaxies are taken from the smaller subsection of the UDS field imaged by The Chandra X-ray survey, whereas the variable sample is taken from the entire UDS field. Attached histograms show the mass and redshift distributions and are normalised.*

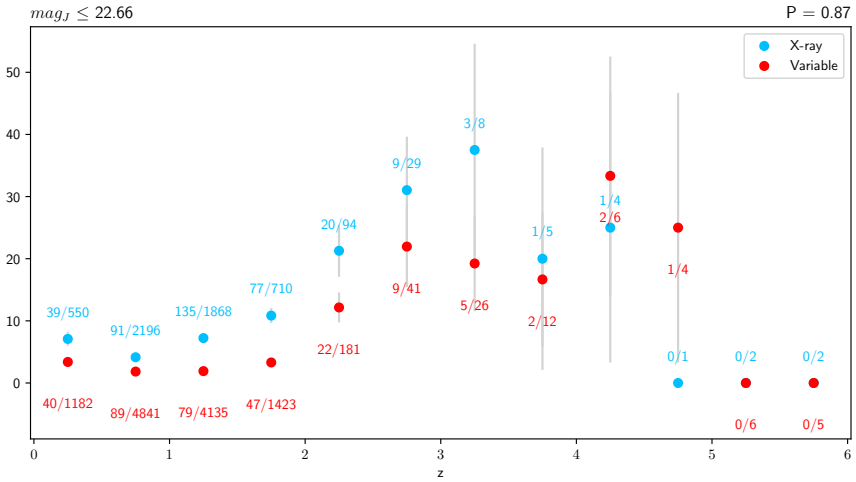

Figure 4.8: *AGN fraction over cosmic time for galaxies with $log(M_*/M_\odot) \geq 10$ and $m_J \leq 22.66$. Bins have a width of Δz=0.5, with red points indicating variability selected AGN fractions and blue points indicating X-ray bright active galaxy fractions, accompanied by binomial errors. Numbered fractions are included with colours corresponding to AGN detection type, with the numerator showing the number of AGN in each bin and the denominator showing the total number of galaxies in each bin. The included P-value comes from a KS test and shows that both samples have statistically similar underlying distributions.*

our sample regardless of their selection method.

Both mass and redshift could be the dominant feature in triggering AGN activity, so to ascertain the main variable that is responsible for the observed trend we looked at the distribution of the AGN fraction on the mass-z plane. Visually, figure 4.9 shows no sign of the horizontal or vertical stripes in colour one would expect if one variable dominated over the other (i.e vertical stripes if AGN are more common at certain epochs regardless of mass or horizontal stripes if AGN are more prevalent in certain mass ranges regardless of the cosmic era).

Utilising principal component analysis to characterise the spread in AGN activity over time, we find the maximum variance in the data is linked more strongly to redshift than mass for both X-ray and variable AGN. This hints that an external process could be the primary trigger for black hole accretion in seemingly any galaxy.

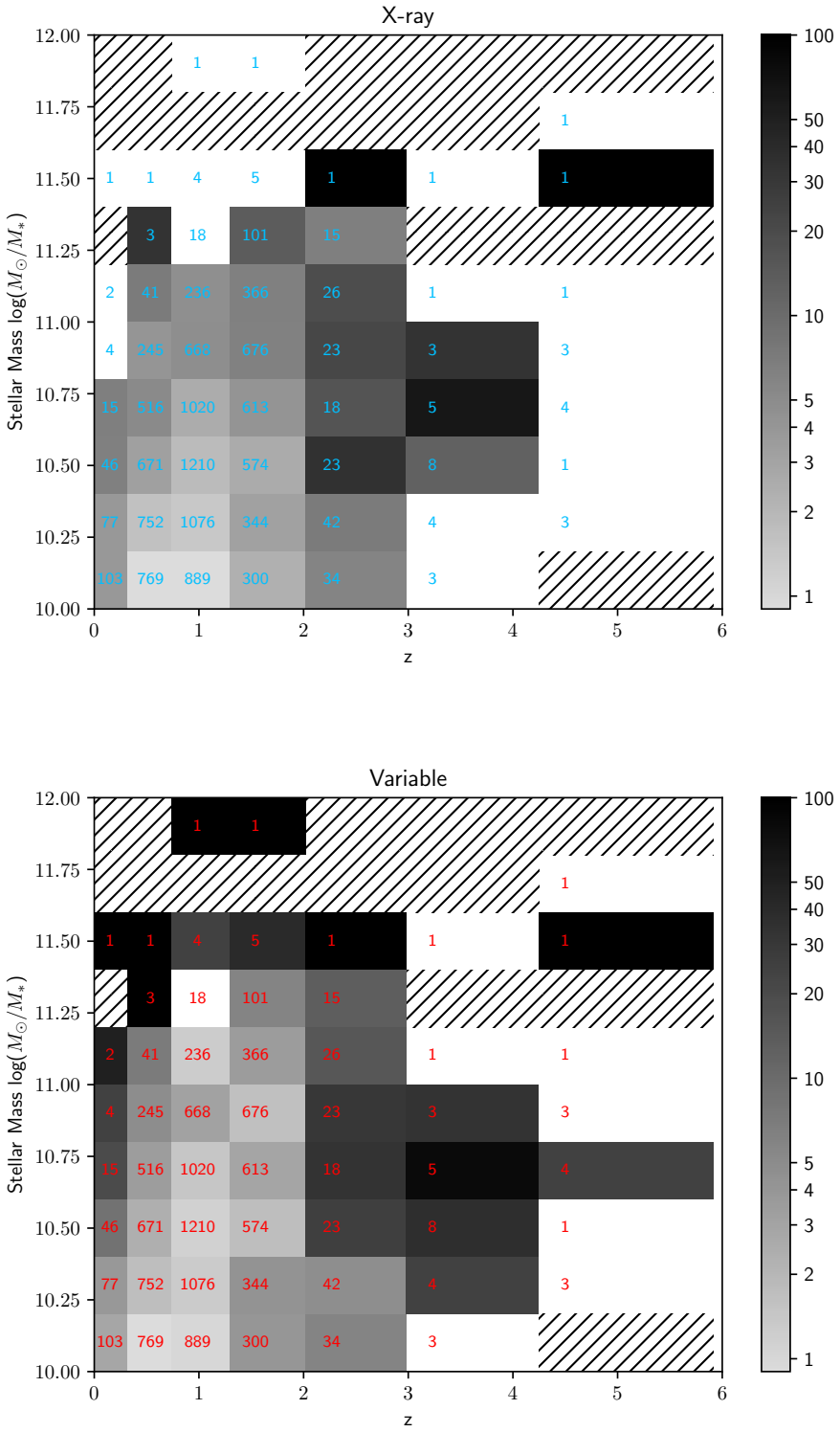

Figure 4.9: *2D histogram of mass vs redshift for galaxies with $log(M_*/M_\odot) \geq 10$ and $m_J \leq 22.66$, colour-coded by the fraction of AGN in each bin for X-ray bright active galaxies (left) and variability selected active galaxies (right). Bin widths are sized according to $\Delta log(M_*/M\odot)$=0.2 and Δz=log(1+z), with each bin having the total number of galaxies denoted on it. Hashed bins indicate areas of the plot where there are no galaxies ad white bins show areas where the AGN fraction is zero, signifying that all of the galaxies in that bin are quiescent.*

4.1.3 Merger triggered accretion?

Throughout this analysis we find a lack of consistent features in the active galaxies being studied.

The only overarching similarity found is the epoch in which AGN activity is most abundant. This hints to the idea that an external process triggers AGN activity in potentially any galaxy given the required conditions, as this would explain why the bulk properties of these active galaxies are different, but the AGN process occurs within them all and peaks at similar cosmic times.

The most popular non-secular triggering mechanism is galaxy mergers, as this would afford the required material for accretion onto a black hole as well as provide the mechanism for the removal of momentum that would allow accretion to occur ([45]).

To test if mergers are the main trigger behind black hole accretion we use data from Galaxy Zoo visual morphological classifications of a subset of UDS galaxies that is covered in the CANDELS Ultra Deep Field ([41]).

Here we match regular inactive galaxies to the active galaxies in terms of mass and redshift, with us requiring control galaxies to have a mass of $m_{ctrl} = \pm 0.2 m_{AGN}$ and redshift $z_{ctrl} = \pm 0.075(1 + z_{AGN})$.

Comparison of the recorded merger rates of active galaxies and their matched control samples can be seen in figure 4.10. Active galaxies show no more signs of being in a recent merger compared to quiescent galaxies of a similar stellar mass that existed at the same time, indicating mergers and interactions are not the main mechanism that activates AGN in these galaxies.

Further to this in figure 4.11 we compare the merger rates of the active galaxies directly. Again we no significant difference between detection method and disturbed morphological features.

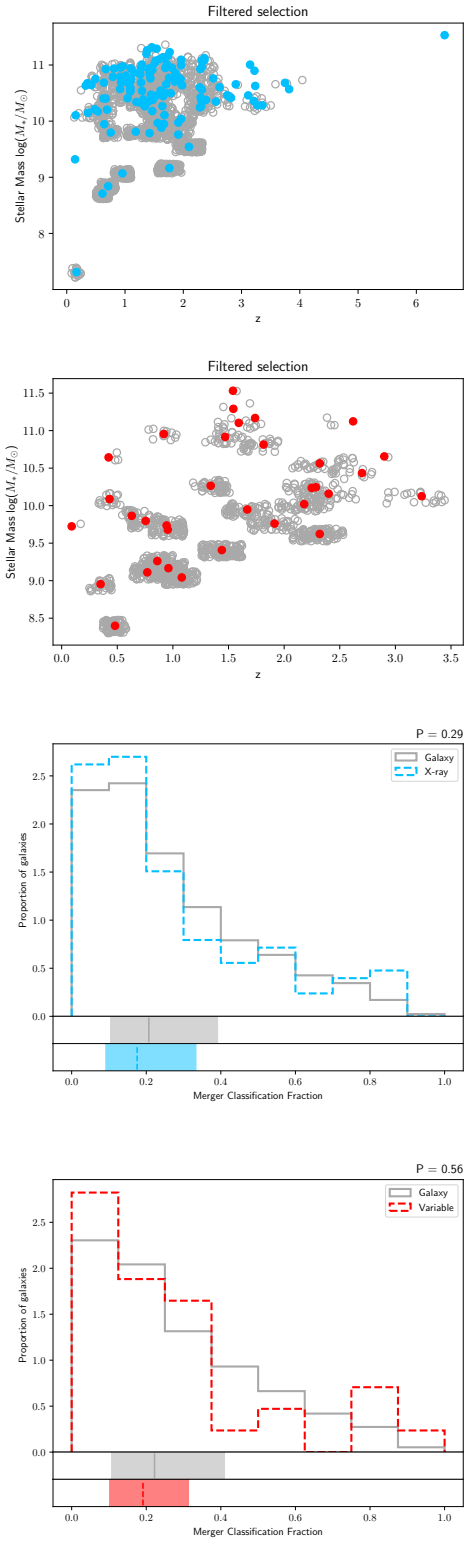

Figure 4.10: *Histograms showing the merger classification fraction of X-ray (left) and variable (right) active galaxies and corresponding control galaxies. Merger classification fraction is the fraction of classifiers who identify merger signs in a given image of a galaxy. For each histogram dashed coloured lines represent active galaxies and grey solid lines represent mass and redshift matched control galaxies. Corresponding coloured horizontal distributions below show the median and interquartile range. P-values come from a KS test between active and control galaxies.*

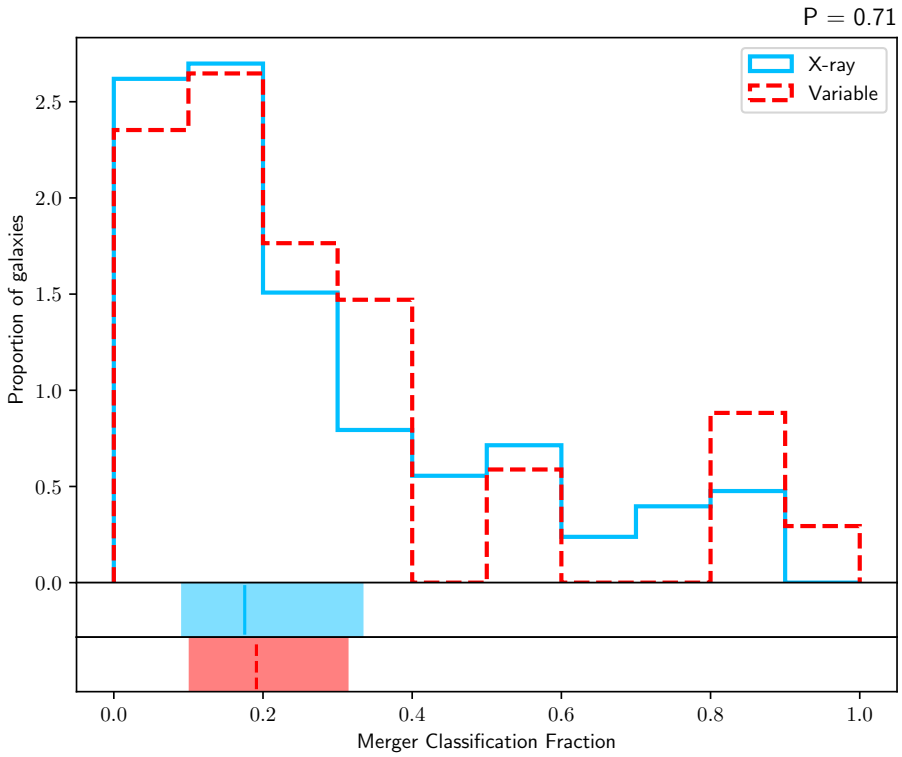

Figure 4.11: *Histograms showing the merger classification fraction of X-ray (blue), dual detected (purple) and variable (red) active galaxies. Coloured horizontal distributions below show median and interquartile range. Merger classification fraction denotes the ratio of classifiers who identify merger signs in a given image of a galaxy. A KS test finds that only variable (red) and dual detected (purple) active galaxies are drawn from different underlying distributions, with a P-value of* $P_v^{xv} = 0.02$.

4.1.4 AGN environment

To investigate if the environment plays a role in triggering the accretion process and igniting AGN activity we study the environment of the active galaxies. We analyse the environmental number density, ρ_{250}, of the active galaxies across all epochs by making use of the nearest neighbour measure within a cylindrical volume around a given galaxy. The dimensions of this volume, is 250kPc in radius and $\pm$0.5GYr in "height" ([42]).

Once again we select a set of control galaxies for each type of active galaxy matched in terms of redshift and stellar mass. We are able to apply stricter filtering in this case as we have environmental measurements for the entire UDS field, not just the spaced based CANDELS UDS field the merger analysis was restricted to. As such our new selection criteria is $m_{ctrl} = \pm 0.2 m_{AGN}$, $z_{ctrl} = \pm 0.025(1 + z_{AGN})$.

We calculate the average environmental density for each group in figure 4.12 and find that X-ray bright active galaxies tend to be in denser environments compared to their quiescent counterparts, however this trend is not present in AGN detected by variability. Further to this direct comparison of the environments of the active galaxies in figure 4.13 shows no significant or consistent differences.

4.2 Discussion

In this research we use long term near infra-red variability measures from The Ultra Deep Survey and find AGN in galaxies previously thought to be dormant. We then use deep Chandra X-ray data to select a set of X-ray bright active galaxies as a comparative sample. Using this data we study the the structure of active galaxies and abundance of AGN activity through cosmic history.

In order to understand the AGN phenomenon as a whole, we compare the similarities and differences in structural parameters, morphology, environment and abundance over time of the new sample of IR variable active galaxies to

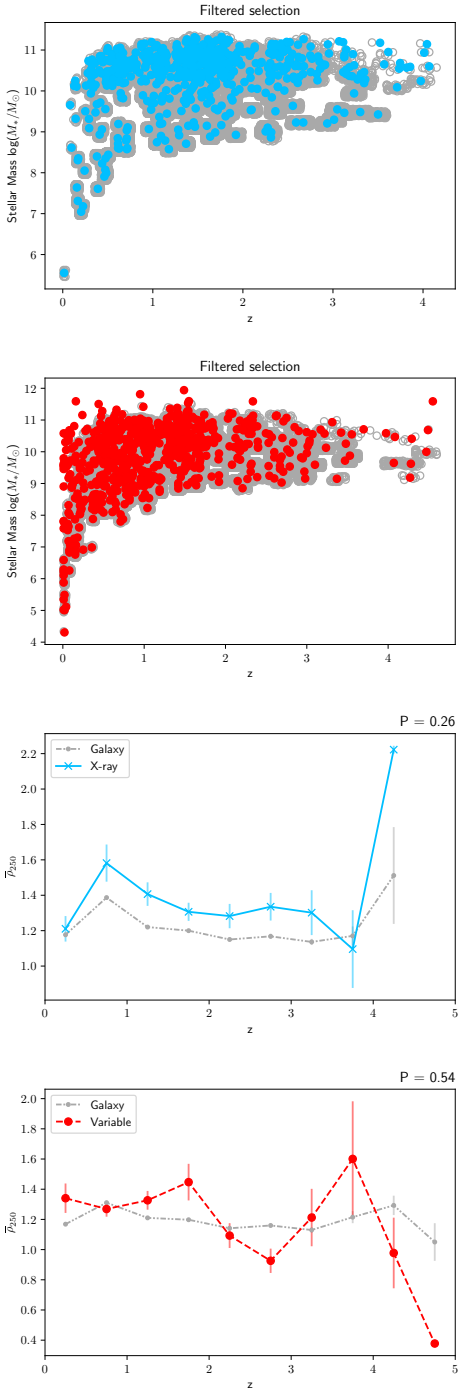

Figure 4.12: *Average environmental density vs redshift for X-ray (left) and variable (right) active galaxies and matched control galaxies. Coloured lines represent active galaxies and grey lines represent mass and redshift matched, inactive control galaxies. Errors on the points are the standard error on the mean. Bins widths are* $\Delta z = 0.5$.

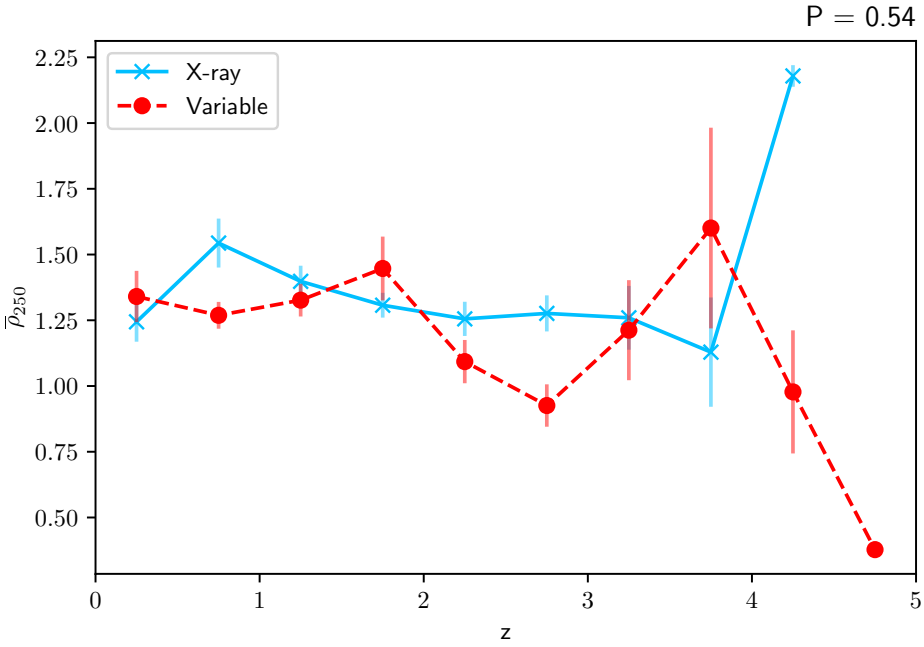

Figure 4.13: *Average environmental density vs redshift for X-ray (blue) and variable (red) active galaxies. Errors are standard errors on the mean. Bins widths are* $\Delta z = 0.5$.

that of AGN found using deep X-ray imaging as well as to regular inactive galaxies.

We first find that IR variability is able to detect AGN in galaxies that are largely missed even in extensive X-ray surveys. We report that for the same area of sky, the fraction of IR variable AGN detected by X-ray emission is 37%. Further to this contrasting X-ray to optical luminosity ratios confirms these objects are truly a new sample of X-ray quiet active galaxies.

Stellar mass measures shows that the variability method probes AGN activity in low mass galaxies that are largely missed by X-ray detection methods. The variable AGN hosts tend to be diskier in morphology and smaller in radial size compared to their X-ray bright counterparts. This is consistent with the expected features when comparing low and high mass galaxies.

We next examined how the abundance of AGN in the universe changed over cosmic time. Selecting a consistent mass range ($\log(M_*/M\odot) \geq 10$) and filtering out low luminosity objects ($m_J \leq 22.66$) such that detections are trustworthy finds that AGN activity peaks at $z \approx 3$. The exact cause of this remains

uncertain, but principal component analysis links this affect to redshift.

The lack of similar physical traits combined with activity peaking at the same epoch for all galaxies favours external processes as triggers for AGN activity over secular effects.

Investigating this through comparison of recent merger features to that of matched, quiescent control galaxies and examining the environment of the active galaxies, however, does not find significant evidence that mergers are a trigger for AGN activity. Instead we find that X-ray active galaxies tend to be in denser environments compared to their dormant counterparts.

Overall we conclude that AGN activity presents as a stochastic process that has the potential to occur in the evolution of any galaxy, but this activity was more common in the early universe. We do not find mergers to be a likely mechanism in the triggering of AGN activity in these galaxies. We show that NIR variability can detect AGN activity in galaxies missed by deep X-ray surveys and that these objects are truly a different set of newly detected AGN. We find that different detection methods have the ability to find AGN in galaxies with different properties and as such to gain a full and complete overview of AGN in the universe at any given time, multiple detection methods should be employed.

4.2.1 Future Work

Ir variability probes the hottest part of the dusty torus of AGN as it falls into the accretion disk. Due to the nature of variability techniques in AGN studies, this means we have been able to study the structure of AGN in galaxies that are currently too far to resolve. Combining this with X-ray measures, which is believed to be generated in the corona of AGN, allows us to research the extremes of the system. This work will be presented in the future.

With next generation instruments such a JWST and accompanying X-ray imaging, the research presented here would be repeatable if a long term survey

is to take place during the lifetime of the telescope. The increased imaging quality would allow for the study of AGN even earlier in the universe.

Chapter 5

Title of Your Third Technical Chapter

5.1 Introduction

Please briefly introduce the motivations, research questions and/or objectives, and indicate your main contributions of this chapter.

[Important] If the page break is not working normally, you can try the command *clearpage*.

5.2 Methodology

5.3 Experimental Results

5.3.1 Dataset

5.3.2 Implementation Details

5.3.3 Evaluation Metrics

5.3.4 Quantitative Results

5.3.5 Qualitative Results

5.4 Discussions

5.4.1 Effectiveness of Each Component

5.4.2 Advantages Compared with Other Algorithms

5.4.3 Limitations and Future Work

5.5 Concluding Remarks

Chapter 6

Title of Your Fourth Technical Chapter or The Application

6.1 Introduction

Please briefly introduce the motivations, research questions and/or objectives, and indicate your main contributions of this chapter.

[Important] If the page break is not working normally, you can try the command *clearpage*.

6.2 Methodology

6.3 Experimental Results

6.3.1 Dataset

6.3.2 Implementation Details

6.3.3 Evaluation Metrics

6.3.4 Quantitative Results

6.3.5 Qualitative Results

6.4 Discussions

6.4.1 Effectiveness of Each Component

6.4.2 Advantages Compared with Other Algorithms

6.4.3 Limitations and Future Work

6.5 Concluding Remarks

Chapter 7

Conclusion

7.1 Main Contributions

Briefly review your main contributions of each chapter or the entire thesis.

7.2 Limitations and Suggestions for Further Improvements

Indicate the limitations and the possible directions of improvements.

7.3 Summary

Finally summarise your thesis.

Bibliography

[1] E. M. Cackett, M. C. Bentz, and E. Kara, "Reverberation mapping of active galactic nuclei: From X-ray corona to dusty torus," *iScience*, vol. 24, no. 6, p. 102557, Jun. 2021. [Online]. Available: https://www.sciencedirect.com/science/article/pii/S2589004221005253

[2] J. Kormendy and D. Richstone, "Inward Bound—The Search for Supermassive Black Holes in Galactic Nuclei," *Annual Review of Astronomy and Astrophysics*, vol. 33, no. 1, pp. 581–624, 1995, _eprint: https://doi.org/10.1146/annurev.aa.33.090195.003053. [Online]. Available: https://doi.org/10.1146/annurev.aa.33.090195.003053

[3] M. B. Eide, B. Ciardi, L. Graziani, P. Busch, Y. Feng, and T. Di Matteo, "Large-scale simulations of H and He reionization and heating driven by stars and more energetic sources," *Monthly Notices of the Royal Astronomical Society*, vol. 498, no. 4, pp. 6083–6099, Oct. 2020. [Online]. Available: https://doi.org/10.1093/mnras/staa2774

[4] J. Kormendy and L. C. Ho, "Coevolution (Or Not) of Supermassive Black Holes and Host Galaxies," *Annual Review of Astronomy and Astrophysics*, vol. 51, no. 1, pp. 511–653, 2013, _eprint: https://doi.org/10.1146/annurev-astro-082708-101811. [Online]. Available: https://doi.org/10.1146/annurev-astro-082708-101811

[5] D. J. Croton, V. Springel, S. D. M. White, G. De Lucia, C. S. Frenk, L. Gao, A. Jenkins, G. Kauffmann, J. F. Navarro, and N. Yoshida, "The many lives of active galactic nuclei: cooling flows, black holes and the luminosities and colours of galaxies," *Monthly Notices of the Royal Astronomical Society*, vol. 365, no. 1, pp. 11–28, Jan. 2006. [Online]. Available: https://doi.org/10.1111/j.1365-2966.2005.09675.x

[6] P. Padovani, D. M. Alexander, R. J. Assef, B. De Marco, P. Giommi, R. C. Hickox, G. T. Richards, V. Smolčić, E. Hatziminaoglou, V. Mainieri, and M. Salvato, "Active galactic nuclei: what's in a name?" *The Astronomy and Astrophysics Review*, vol. 25, no. 1, p. 2, Aug. 2017. [Online]. Available: https://doi.org/10.1007/s00159-017-0102-9

[7] N. A. Grogin, C. J. Conselice, E. Chatzichristou, D. M. Alexander, F. E. Bauer, A. E. Hornschemeier, S. Jogee, A. M. Koekemoer, V. G. Laidler, M. Livio, R. A. Lucas, M. Paolillo, S. Ravindranath, E. J. Schreier, B. D. Simmons, and C. M. Urry, "AGN Host Galaxies at z ˜ 0.4-1.3: Bulge-dominated and Lacking Merger-AGN Connection," *The Astrophysical Journal*, vol. 627, no. 2, p.

L97, Jun. 2005, publisher: IOP Publishing. [Online]. Available: https://iopscience.iop.org/article/10.1086/432256/meta

[8] J. M. Gabor, C. D. Impey, K. Jahnke, B. D. Simmons, J. R. Trump, A. M. Koekemoer, M. Brusa, N. Cappelluti, E. Schinnerer, V. Smolčić, M. Salvato, J. D. Rhodes, B. Mobasher, P. Capak, R. Massey, A. Leauthaud, and N. Scoville, "ACTIVE GALACTIC NUCLEUS HOST GALAXY MORPHOLOGIES IN COSMOS*," *The Astrophysical Journal*, vol. 691, no. 1, p. 705, Jan. 2009, publisher: The American Astronomical Society. [Online]. Available: https://dx.doi.org/10.1088/0004-637X/691/1/705

[9] C. M. Pierce, J. M. Lotz, J. R. Primack, D. J. V. Rosario, R. L. Griffith, C. J. Conselice, S. M. Faber, D. C. Koo, A. L. Coil, S. Salim, A. M. Koekemoer, E. S. Laird, R. J. Ivison, and R. Yan, "The effects of an active galactic nucleus on host galaxy colour and morphology measurements," *Monthly Notices of the Royal Astronomical Society*, vol. 405, no. 2, pp. 718–734, Jun. 2010. [Online]. Available: https://doi.org/10.1111/j.1365-2966.2010.16502.x

[10] L. Fan, G. Fang, Y. Chen, J. Li, X. Lv, K. K. Knudsen, and X. Kong, "STRUCTURE AND MORPHOLOGY OF X-RAY-SELECTED ACTIVE GALACTIC NUCLEUS HOSTS AT $1 < z < 3$ IN THE CANDELS-COSMOS FIELD," *The Astrophysical Journal Letters*, vol. 784, no. 1, p. L9, Mar. 2014, publisher: The American Astronomical Society. [Online]. Available: https://dx.doi.org/10.1088/2041-8205/784/1/L9

[11] D. B. Sanders, B. T. Soifer, J. H. Elias, B. F. Madore, K. Matthews, G. Neugebauer, and N. Z. Scoville, "Ultraluminous Infrared Galaxies and the Origin of Quasars," *The Astrophysical Journal*, vol. 325, p. 74, Feb. 1988, aDS Bibcode: 1988ApJ...325...74S. [Online]. Available: https://ui.adsabs.harvard.edu/abs/1988ApJ...325...74S

[12] P. F. Hopkins, L. Hernquist, T. J. Cox, T. D. Matteo, B. Robertson, and V. Springel, "A Unified, Merger-driven Model of the Origin of Starbursts, Quasars, the Cosmic X-Ray Background, Supermassive Black Holes, and Galaxy Spheroids," *The Astrophysical Journal Supplement Series*, vol. 163, no. 1, p. 1, Mar. 2006, publisher: IOP Publishing. [Online]. Available: https://iopscience.iop.org/article/10.1086/499298/meta

[13] T. Urrutia, M. Lacy, and R. H. Becker, "Evidence for Quasar Activity Triggered by Galaxy Mergers in HST Observations of Dust-reddened Quasars," *The Astrophysical Journal*, vol. 674, no. 1, p. 80, Feb. 2008, publisher: IOP Publishing. [Online]. Available: https://iopscience.iop.org/article/10.1086/523959/meta

[14] P. F. Hopkins, L. Hernquist, T. J. Cox, and D. Kereš, "A Cosmological Framework for the Co-Evolution of Quasars, Supermassive Black Holes, and Elliptical Galaxies. I. Galaxy Mergers and Quasar Activity," *The Astrophysical Journal Supplement Series*, vol. 175, no. 2, p.

356, Apr. 2008, publisher: IOP Publishing. [Online]. Available: https://iopscience.iop.org/article/10.1086/524362/meta

[15] J. C. S. Pierce, C. Tadhunter, C. Ramos Almeida, P. Bessiere, J. V. Heaton, S. L. Ellison, G. Speranza, Y. Gordon, C. O'Dea, L. Grimmett, and L. Makrygianni, "Galaxy interactions are the dominant trigger for local type 2 quasars," *Monthly Notices of the Royal Astronomical Society*, vol. 522, no. 2, pp. 1736–1751, Jun. 2023. [Online]. Available: https://doi.org/10.1093/mnras/stad455

[16] M. Cisternas, K. Jahnke, K. J. Inskip, J. Kartaltepe, A. M. Koekemoer, T. Lisker, A. R. Robaina, M. Scodeggio, K. Sheth, J. R. Trump, R. Andrae, T. Miyaji, E. Lusso, M. Brusa, P. Capak, N. Cappelluti, F. Civano, O. Ilbert, C. D. Impey, A. Leauthaud, S. J. Lilly, M. Salvato, N. Z. Scoville, and Y. Taniguchi, "THE BULK OF THE BLACK HOLE GROWTH SINCE z 1 OCCURS IN A SECULAR UNIVERSE: NO MAJOR MERGER–AGN CONNECTION*," *The Astrophysical Journal*, vol. 726, no. 2, p. 57, Dec. 2010, publisher: The American Astronomical Society. [Online]. Available: https://dx.doi.org/10.1088/0004-637X/726/2/57

[17] T. Kawaguchi, S. Mineshige, M. Umemura, and E. L. Turner, "Optical Variability in Active Galactic Nuclei: Starbursts or Disk Instabilities?" *The Astrophysical Journal*, vol. 504, no. 2, p. 671, Sep. 1998, publisher: IOP Publishing. [Online]. Available: https://iopscience.iop.org/article/10.1086/306105/meta

[18] D. E. V. Berk, B. C. Wilhite, R. G. Kron, S. F. Anderson, R. J. Brunner, P. B. Hall, Ivezić, G. T. Richards, D. P. Schneider, D. G. York, J. V. Brinkmann, D. Q. Lamb, R. C. Nichol, and D. J. Schlegel, "The Ensemble Photometric Variability of ˜25,000 Quasars in the Sloan Digital Sky Survey," *The Astrophysical Journal*, vol. 601, no. 2, p. 692, Feb. 2004, publisher: IOP Publishing. [Online]. Available: https://iopscience.iop.org/article/10.1086/380563/meta

[19] A. V. Filippenko, "The "Seyfert 1" Optical Spectra of the Type II Supernovae 1987F and 1988I," *The Astronomical Journal*, vol. 97, p. 726, Mar. 1989, aDS Bibcode: 1989AJ.....97..726F. [Online]. Available: https://ui.adsabs.harvard.edu/abs/1989AJ.....97..726F

[20] R. Terlevich, G. Tenorio-Tagle, J. Franco, and J. Melnick, "The starburst model for active galactic nuclei: the broad-line region as supernova remnants evolving in a high-density medium," *Monthly Notices of the Royal Astronomical Society*, vol. 255, no. 4, pp. 713–728, Apr. 1992. [Online]. Available: https://doi.org/10.1093/mnras/255.4.713

[21] M. Hawkins, "Variability in active galactic nuclei: confrontation of models with observations," *Monthly Notices of the Royal Astronomical Society*, vol. 329, no. 1, pp. 76–86, Jan. 2002. [Online]. Available: https://doi.org/10.1046/j.1365-8711.2002.04939.x

[22] I. Aretxaga, R. C. Femandes, Jr, and R. J. Terlevich, "QSO variability: probing the starburst model," *Monthly Notices of the Royal Astronomical Society*, vol. 286, no. 2, pp. 271–283, Apr. 1997. [Online]. Available: https://doi.org/10.1093/mnras/286.2.271

[23] T. J. L. Courvoisier, S. Paltani, and R. Walter, "Are active galactic nuclei powered by stellar collisions?" *Astronomy and Astrophysics*, vol. 308, pp. L17–L20, Apr. 1996, aDS Bibcode: 1996A&A...308L..17C. [Online]. Available: https://ui.adsabs.harvard.edu/abs/1996A&A...308L..17C

[24] G. Torricelli-Ciamponi, C. Foellmi, T. J. L. Courvoisier, and S. Paltani, "Can star collisions explain the AGN variability?" *Astronomy and Astrophysics*, vol. 358, pp. 57–64, Jun. 2000, aDS Bibcode: 2000A&A...358...57T. [Online]. Available: https://ui.adsabs.harvard.edu/abs/2000A&A...358...57T

[25] M. Hawkins, "Dark Matter from Quasar Microlensing," *Annals of the New York Academy of Sciences*, vol. 759, no. 1, pp. 596–599, 1995, _eprint: https://onlinelibrary.wiley.com/doi/pdf/10.1111/j.1749-6632.1995.tb17616.x. [Online]. Available: https://onlinelibrary.wiley.com/doi/abs/10.1111/j.1749-6632.1995.tb17616.x

[26] J. Aird, A. L. Coil, A. Georgakakis, K. Nandra, G. Barro, and P. G. Pérez-González, "The evolution of the X-ray luminosity functions of unabsorbed and absorbed AGNs out to z 5," *Monthly Notices of the Royal Astronomical Society*, vol. 451, no. 2, pp. 1892–1927, Aug. 2015. [Online]. Available: https://doi.org/10.1093/mnras/stv1062

[27] P. Sánchez, P. Lira, R. Cartier, V. Pérez, N. Miranda, C. Yovaniniz, P. Arévalo, B. Milvang-Jensen, J. Fynbo, J. Dunlop, P. Coppi, and S. Marchesi, "Near-infrared Variability of Obscured and Unobscured X-Ray-selected AGNs in the COSMOS Field," *The Astrophysical Journal*, vol. 849, no. 2, p. 110, Nov. 2017, publisher: The American Astronomical Society. [Online]. Available: https://dx.doi.org/10.3847/1538-4357/aa9188

[28] R. M. Cutri, W. Z. Wisniewski, G. H. Rieke, and M. J. Lebofsky, "Variability and the nature of QSO optical-infrared continua." *The Astrophysical Journal*, vol. 296, pp. 423–429, Sep. 1985, aDS Bibcode: 1985ApJ...296..423C. [Online]. Available: https://ui.adsabs.harvard.edu/abs/1985ApJ...296..423C

[29] P. Lira, P. Arévalo, P. Uttley, I. McHardy, and E. Breedt, "Optical and near-IR long-term monitoring of NGC 3783 and MR 2251178: evidence for variable near-IR emission from thin accretion discs," *Monthly Notices of the Royal Astronomical Society*, vol. 415, no. 2, pp. 1290–1303, Aug. 2011. [Online]. Available: https://doi.org/10.1111/j.1365-2966.2011.18774.x

[30] P. Lira, P. Arévalo, P. Uttley, I. M. M. McHardy, and L. Videla, "Long-term monitoring of the archetype Seyfert galaxy MCG-6-30-15: X-ray, optical and near-IR variability of the corona, disc and torus," *Monthly*

Notices of the Royal Astronomical Society, vol. 454, no. 1, pp. 368–379, Nov. 2015. [Online]. Available: https://doi.org/10.1093/mnras/stv1945

[31] S. Kouzuma and H. Yamaoka, "ENSEMBLE VARIABILITY OF NEAR-INFRARED-SELECTED ACTIVE GALACTIC NUCLEI," *The Astrophysical Journal*, vol. 747, no. 1, p. 14, Feb. 2012, publisher: The American Astronomical Society. [Online]. Available: https://dx.doi.org/10.1088/0004-637X/747/1/14

[32] S. Son, M. Kim, and L. C. Ho, "Mid-infrared Variability of Low-redshift Active Galactic Nuclei: Constraints on a Hot Dust Component with a Variable Covering Factor," *The Astrophysical Journal*, vol. 927, no. 1, p. 107, Mar. 2022, publisher: The American Astronomical Society. [Online]. Available: https://dx.doi.org/10.3847/1538-4357/ac4dfc

[33] R. A. Edelson and M. A. Malkan, "Far-Infrared Variability in Active Galactic Nuclei," *The Astrophysical Journal*, vol. 323, p. 516, Dec. 1987, aDS Bibcode: 1987ApJ...323..516E. [Online]. Available: https://ui.adsabs.harvard.edu/abs/1987ApJ...323..516E

[34] G. Neugebauer, B. T. Soifer, K. Matthews, and J. H. Elias, "The Near-Infrared Variability of a Sample of Optically Selected Quasars," *The Astronomical Journal*, vol. 97, p. 957, Apr. 1989, aDS Bibcode: 1989AJ.....97..957N. [Online]. Available: https://ui.adsabs.harvard.edu/abs/1989AJ.....97..957N

[35] E. Elmer, O. Almaini, M. Merrifield, W. G. Hartley, D. T. Maltby, A. Lawrence, I. Botti, and P. Hirst, "Long-term NIR variability in the UKIDSS Ultra Deep Survey: a new probe of AGN activity at high redshift," *Monthly Notices of the Royal Astronomical Society*, vol. 493, no. 2, pp. 3026–3035, Apr. 2020. [Online]. Available: https://doi.org/10.1093/mnras/staa381

[36] D. D. Kocevski, G. Hasinger, M. Brightman, K. Nandra, A. Georgakakis, N. Cappelluti, F. Civano, Y. Li, Y. Li, J. Aird, D. M. Alexander, O. Almaini, M. Brusa, J. Buchner, A. Comastri, C. J. Conselice, M. A. Dickinson, A. Finoguenov, R. Gilli, A. M. Koekemoer, T. Miyaji, J. R. Mullaney, C. Papovich, D. Rosario, M. Salvato, J. D. Silverman, R. S. Somerville, and Y. Ueda, "X-UDS: The Chandra Legacy Survey of the UKIDSS Ultra Deep Survey Field," *The Astrophysical Journal Supplement Series*, vol. 236, no. 2, p. 48, Jun. 2018, publisher: The American Astronomical Society. [Online]. Available: https://dx.doi.org/10.3847/1538-4365/aab9b4

[37] C. Simpson, A. Martínez-Sansigre, S. Rawlings, R. Ivison, M. Akiyama, K. Sekiguchi, T. Takata, Y. Ueda, and M. Watson, "Radio imaging of the Subaru/XMM–Newton Deep Field – I. The 100-Jy catalogue, optical identifications, and the nature of the faint radio source population," *Monthly Notices of the Royal Astronomical Society*, vol. 372, no. 2, pp. 741–757, Oct. 2006. [Online]. Available: https://doi.org/10.1111/j.1365-2966.2006.10907.x

[38] C. Simpson, P. Westoby, V. Arumugam, R. Ivison, W. Hartley, and O. Almaini, "The prevalence of AGN feedback in massive galaxies at z 1," *Monthly Notices of the Royal Astronomical Society*, vol. 433, no. 3, pp. 2647–2656, Aug. 2013. [Online]. Available: https://doi.org/10.1093/mnras/stt940

[39] G. Bruzual and S. Charlot, "Stellar population synthesis at the resolution of 2003," *Monthly Notices of the Royal Astronomical Society*, vol. 344, no. 4, pp. 1000–1028, Oct. 2003. [Online]. Available: https://doi.org/10.1046/j.1365-8711.2003.06897.x

[40] G. B. Brammer, P. G. v. Dokkum, and P. Coppi, "EAZY: A Fast, Public Photometric Redshift Code," *The Astrophysical Journal*, vol. 686, no. 2, p. 1503, Oct. 2008, publisher: IOP Publishing. [Online]. Available: https://iopscience.iop.org/article/10.1086/591786/meta

[41] B. D. Simmons, C. Lintott, K. W. Willett, K. L. Masters, J. S. Kartaltepe, B. Häußler, S. Kaviraj, C. Krawczyk, S. J. Kruk, D. H. McIntosh, R. J. Smethurst, R. C. Nichol, C. Scarlata, K. Schawinski, C. J. Conselice, O. Almaini, H. C. Ferguson, L. Fortson, W. Hartley, D. Kocevski, A. M. Koekemoer, A. Mortlock, J. A. Newman, S. P. Bamford, N. A. Grogin, R. A. Lucas, N. P. Hathi, E. McGrath, M. Peth, J. Pforr, Z. Rizer, S. Wuyts, G. Barro, E. F. Bell, M. Castellano, T. Dahlen, A. Dekel, J. Ownsworth, S. M. Faber, S. L. Finkelstein, A. Fontana, A. Galametz, R. Grützbauch, D. Koo, J. Lotz, B. Mobasher, M. Mozena, M. Salvato, and T. Wiklind, "Galaxy Zoo: quantitative visual morphological classifications for 48 000 galaxies from CANDELS," *Monthly Notices of the Royal Astronomical Society*, vol. 464, no. 4, pp. 4420–4447, Feb. 2017. [Online]. Available: https://doi.org/10.1093/mnras/stw2587

[42] C. Lani, O. Almaini, W. G. Hartley, A. Mortlock, B. Häußler, R. W. Chuter, C. Simpson, A. van der Wel, R. Grützbauch, C. J. Conselice, E. J. Bradshaw, M. C. Cooper, S. M. Faber, N. A. Grogin, D. D. Kocevski, A. M. Koekemoer, and K. Lai, "Evidence for a correlation between the sizes of quiescent galaxies and local environment to z 2," *Monthly Notices of the Royal Astronomical Society*, vol. 435, no. 1, pp. 207–221, Oct. 2013. [Online]. Available: https://doi.org/10.1093/mnras/stt1275

[43] O. Almaini, A. Lawrence, T. Shanks, A. Edge, B. J. Boyle, I. Georgantopoulos, K. F. Gunn, G. C. Stewart, and R. E. Griffiths, "X-ray variability in a deep, flux-limited sample of QSOs," *Monthly Notices of the Royal Astronomical Society*, vol. 315, no. 2, pp. 325–336, Jun. 2000. [Online]. Available: https://doi.org/10.1046/j.1365-8711.2000.03385.x

[44] P. Madau and M. Dickinson, "Cosmic Star-Formation History," *Annual Review of Astronomy and Astrophysics*, vol. 52, no. 1, pp. 415–486, 2014, _eprint: https://doi.org/10.1146/annurev-astro-081811-125615. [Online]. Available: https://doi.org/10.1146/annurev-astro-081811-125615

[45] G. Canalizo and A. Stockton, "Quasi-Stellar Objects, Ultraluminous Infrared Galaxies, and Mergers*," *The Astrophysical Journal*, vol. 555,

no. 2, p. 719, Jul. 2001, publisher: IOP Publishing. [Online]. Available: https://iopscience.iop.org/article/10.1086/321520/meta

Appendix A

List of Abbreviations

CNN	Convolutional Neural Network
DCNN	Deep Convolutional Neural Network
RNN	Recurrent Neural Network
LSTM	Long-Short Term Memory
GAN	Generative Adversarial network
SAE	Stacked Auto Encoder
RCL	Recurrent Convolutional Layers
LRN	Local Response Normalization
FC	Fully Connection
RBM	Restricted Boltzmann Machine
CRF	Conditional Random Fields
SOD	Salient Object Detection
PCA	Principal Component Analysis
HOG	Histogram of Oriented Gradients
LBP	Local Binary Pattern
SVM	Support Vector Machine
CorLoc	Correct Localization
IoU	Intersection over Union
mAP	mean Average Precision
mAR	mean Average Recall
MAE	Mean Average Error
PR	Precision-Recall
TP	True Positive
TN	True Negative
FP	False Positive
FN	False Negative
KC	Kappa Coefficient
OE	Overall Error
CA	Classification Accuracy
UAV	Unmanned Aerial Vehicles
SAR	Synthetic Aperture Radar